On the missing momentum dependence of the color transparency effects in $(e, e'p)$ scattering

O.Benhar[1], S.Fantoni[2,3], N.N.Nikolaev[4,5], J.Speth[4], A.A.Usmani[2], B.G.Zakharov[5]

[1] *INFN, Sezione Sanità, Physics Laboratory, Istituto Superiore di Sanità. I-00161 Roma, Italy*

[2] *Interdisciplinary Laboratory, SISSA, INFN, Sezione di Trieste. I-34014, Trieste, Italy*

[3] *International Centre for Theoretical Physics, Strada Costiera 11, I-34014, Trieste, Italy*

[4] *IKP(Theorie), Forschungszentrum Jülich GmbH.*

D-52425 Jülich, Germany

[5] *L.D.Landau Institute for Theoretical Physics,*

GSP-1, 117940, ul.Kosygina 2., V-334 Moscow, Russia

(February 9, 2008)

Abstract

We explore the missing momentum dependence of the CT effects in quasielastic $(e, e'p)$ scattering. We develop the coupled-channel multiple-scattering theory (CCMST) description of final-state interaction including both the coherent and incoherent rescatterings of the ejectile state. We demonstrate that the contribution of the off-diagonal incoherent rescattering does not vanish at low Q^2 which is a novel correction to the conventional Glauber theory evaluation of nuclear transparency. We comment on the nontrivial impact of this correction on the onset of CT. The sensitivity of the onset of CT to the $3q$-nucleon reggeon amplitudes is discussed for the first time. We present numerical results for nuclear transparency as a function of the missing momentum for exclusive $(e, e'p)$ reaction in the kinematical region of $Q^2 \lesssim 40$ GeV^2 and $p_m \lesssim 250$ MeV/c. Our evalua-

tions show that at $Q^2 \sim 10$ CT effects are substantial only in antiparallel kinematics at $p_{m,z} \sim -250$ MeV/c. The effect is enhanced on light nuclei and could be observed in a high precision experiment.

I. INTRODUCTION

The quasielastic $(e, e'p)$ reaction plays an important role in the nuclear physics as a tool for investigation of the nuclear structure. At high Q^2 it becomes interesting from the point of view of the particle physics as well. The perturbative QCD [1] suggests that the dominant mechanism of ep scattering at high Q^2 is an interaction of the virtual photon with small-size ($\rho \sim 1/Q$) $3q$ configurations in the proton wave function. It is expected [2,3] that this mechanism should manifest itself through the vanishing of final state interaction (FSI) in $(e, e'p)$ reaction in the limit of high Q^2 because the small-size $3q$ ejectile state formed after absorption of the virtual photon will weakly interact with the spectator nucleons. As a consequence, at high Q^2 the nuclear transparency, T_A, defined as a ratio of the experimentally measured cross section to the theoretical cross section calculated in the plane wave impulse approximation (PWIA) should tend to unity, and the experimental missing momentum distribution be close to the single particle momentum distribution (SPMD) of the proton in the target nucleus. The observation of this effect, which is usually referred to as the color transparency (CT) phenomenon, would be a direct test of the space-time picture of hard processes predicted by perturbative QCD.

An accurate evaluation of FSI effects requires a quantum mechanical treatment of the evolution of the $3q$ ejectile wave function in the nuclear medium. At large Q^2 ($\gtrsim 2$ GeV^2) the kinetic energy of the struck proton $T_{kin} \approx Q^2/2m_p$ (here m_p is the proton mass) becomes large enough for the Glauber-Gribov coupled-channel multiple scattering theory (CCMST) [4,5] to be applicable for this purpose. The CCMST allows one to sum the quantum mechanical amplitudes contributing to electroexcitation and diffractive de-excitation of the struck proton $p \to i_1 \to ... \to i_\nu \to p$ provided that the nucleus wave function, $3q$-nucleon scattering matrix and initial ejectile $3q$ wave function are known. In CCMST the CT phenomenon corresponds to a cancellation between the rescattering amplitudes with elastic (diagonal) and inelastic (off-diagonal) intermediate states. Such a nontrivial cancellation becomes possible in QCD due to the existence of the CT sum

rules [6], which relate diagonal and off-diagonal transition amplitudes.

Several works were devoted to the study of CT effects in $(e, e'p)$ scattering within the coupled-channel formalism under different assumptions for the $3q$-nucleon scattering amplitudes [6–10]. The results of these analyses show that in the case of the integrated nuclear transparency effect of the off-diagonal rescatterings is still small at $Q^2 \lesssim 10$ GeV^2. More recent calculations [11,12] within the Green's function approach developed in refs. [13,14] also yield slow onset of CT. This prediction is consistent with the weak Q^2-dependence of the nuclear transparency observed in the NE18 experiment [15].

FSI effects vary with the missing momentum, $\vec{p}_m$, and CT effects may be enhanced in some kinematical regions. The analyses of refs. [8–10] show that the off-diagonal rescatterings give rise to the forward-backward (F-B) asymmetry of the missing momentum distribution. In the forthcoming high precision experiments at CEBAF, such a F-B asymmetry could have been a better signature of CT than the weak Q^2-dependence of the integrated nuclear transparency. However, the nonzero Re/Im ratio, α_{pN}, for the forward pN scattering amplitude makes the nuclear medium dispersive for the struck proton and leads to a difference between its asymptotic momentum and momentum inside the nucleus. This difference entails a longitudinal shift of the missing momentum distribution and also generates the F-B asymmetry which has not been considered in [8–10]. Within the context of the analysis of the inclusive data from SLAC, the role played by α_{pN} in eA scattering at high Q^2 has been pointed out in ref. [16]. The recent analyses [17,18] demonstrated that the F-B asymmetry, associated with α_{pN}, at $Q^2 \lesssim 10$ GeV^2 is of the same order, or even larger than generated by the CT effects. Besides omitting the large effect of α_{pN} on the F-B asymmetry, CT effects in refs. [8–10] were evaluated under certain qualitative approximations. In ref. [9] the sum of the CCMST series was performed using the approximation of the effective diffraction scattering matrix; ref. [8] has used several unjustified approximations in the numerical calculations, and the authors of ref. [10] have used incorrect initial ejectile $3q$ wave function (for the criticism to the approaches of refs.

[8,10] see [18]). Furthermore, none of refs. [8–10] has discussed the $p_{m\perp}$-dependence of CT effects. On the whole, the theoretical understanding of the $\vec{p}_m$-dependence of CT effects is far from being complete and further investigations of this problem are required.

In the present paper we study the missing momentum dependence of the nuclear transparency in the region of $p_m \lesssim k_F$ (here $k_F \approx 250$ MeV/c is the Fermi momentum). We perform an exact evaluation of CCMST series, thus improving upon the approximation of the effective diffraction matrix [9], and for the first time study the convergence of CCMST expansion in the number of the excited proton states. In our evaluation of CT effects we use the realistic Pomeron part of the $3q$-nucleon diffraction scattering matrix, which was previously used in ref. [6] for calculation of the integrated nuclear transparency. We study the sensitivity of the results to the choice of the reggeon $3q$-nucleon amplitudes.

The present analysis is focused on the use of CCMST to describe the evolution of the $3q$ ejectile state during its propagation through the nuclear medium. We evaluate CCMST series describing the nucleus wave function in the independent particle shell model. The short range correlations (SRC) have been neglected motivated by the relatively small correlation effects on the SPMD [19,20] and on the missing momentum distribution in $^4He(p,2p)$ found in the recent many-body Glauber analysis [21] at $p_m \lesssim k_F$. However in ref. [20], it is observed that NN short range central correlation is responsible for the SPMD tail and that the tensor correlation enhances the tail further almost by a factor of 3 without changing its shape. It is feasible that using Monte Carlo approaches for light nuclei and the local density approximation for heavier systems, one could eventually perform a more sophisticated analysis including SRC.

The coupled channel formalism is developed in a form which includes both the coherent and incoherent rescatterings of the ejectile state in the nuclear medium. In the single-channel Glauber model, the role of the incoherent FSI was elucidated in ref. [17]. It was shown that in the shell model, the allowance for both the coherent and incoherent rescatterings corresponds to the inclusive $(e,e'p)$ reaction, when all the final states of the

residual nucleus are involved, while the cross section obtained neglecting the incoherent rescatterings is related to the exclusive $(e, e'p)$ reaction, when only the one-hole excitations of the target nucleus are allowed. The analysis [17] shows that the incoherent rescatterings become important at $p_m \gtrsim 200 - 250$ MeV/c. The impact of the incoherent off-diagonal rescatterings on the onset of CT has not yet been treated quantitatively. We demonstrate that, on the contrary to the coherent off-diagonal rescatterings, the contribution of the off-diagonal incoherent rescatterings does not vanish at low Q^2. We also show that in the case of incoherent rescatterings the CT effects decrease the nuclear transparency.

The numerical calculations of the present paper are performed for the exclusive $(e, e'p)$ reaction. In the region of the relatively small missing momenta ($p_m \lesssim 150 - 200$ MeV/c), where the contribution of the incoherent rescatterings is negligible, our theoretical predictions may be compared with inclusive experimental data.

The correspondence between the coherent FSI and the one-hole excitations allows an evaluation of the $\vec{p}_m$-dependence of CT effects for different hole states. Because of the change of the spatial distribution of the bound proton, we find significant variations of nuclear transparency from the one hole state to another. We present estimates of CT effects for different acceptance windows in the transverse and longitudinal missing momentum. Previously, different hole excitations were considered in [22] in a model of classical evolution of the ejectile state, which conflicts the coherency properties of CCMST.

The paper is organized as follows. In section 2 we set out the CCMST formalism for $(e, e'p)$ reaction. The emphasis is placed on the approximations which are necessary to obtain the intuitive formula of the optical approximation. The considerations of the parameterization of the diffraction matrix and of the initial ejectile wave function are given in section 3. In section 4 we apply the formalism of CCMST for qualitative analysis of the incoherent FSI. The numerical results obtained for exclusive $^{16}O(e, e'p)$ and $^{40}Ca(e, e'p)$ reactions are presented in section 5. The summary and conclusions are presented in section 6.

II. FSI IN THE GLAUBER-GRIBOV FORMALISM

We begin with the kinematics of quasielastic $(e, e'p)$ scattering. In the present paper we, following the usual practice [23–25], assume that at high Q^2 the differential cross section of $(e, e'p)$ reaction may be expressed through the half off-shell ep-cross section, σ_{ep}, and the distorted spectral function, $S(E_m, \vec{p}_m)$, as

$$\frac{d\sigma}{dQ^2 d\nu dp d\Omega_p} = K \sigma_{ep} S(E_m, \vec{p}_m)\,. \tag{1}$$

Here K is a kinematical factor, ν and $\vec{q}$ are the (e, e') energy and momentum transfer, $Q^2 = \vec{q}^{\,2} - \nu^2$, the struck proton has a momentum $\vec{p}$ and energy $E(p) = T_{kin} + m_p$, the missing momentum and energy are defined as $\vec{p}_m = \vec{q} - \vec{p}$ and $E_m = \nu + m_p - E(p)$ and the z-axis is chosen along $\vec{q}$. Apart from E_m and $\vec{p}_m$ the distorted spectral function depends on $\vec{p}$. In Eq. (1) and hereafter we suppress this variable. Eq. (1) is written under the assumption that the difference between the spectral functions corresponding to absorption of the longitudinal (L) and transverse (T) photons, connected with the spin dependence of FSI and CT effects, can be neglected. We ignore the spin effects in FSI because at large energy of the struck proton they become small. As far as the CT effects are concerned, we will see that in the case of dominance of the small-size $3q$ configurations in hard ep scattering, which is of our interest in the present paper, the contribution of the off-diagonal rescatterings to the longitudinal and transverse spectral functions must be close to each other. Since we do not distinguish the longitudinal and transverse spectral functions, below we treat the electromagnetic current as a scalar operator. Also, notice that Eq. (1) is for the cross section averaged over the azimuthal angle between the missing momentum and the (e, e') reaction plane, which does not contain the LT and TT interference responses [25].

In terms of the distorted spectral function the nuclear transparency for a certain kinematical domain, D, of the missing energy and the missing momentum can be written as

$$T_A(D) = \frac{\int\limits_D dE_m d^3\vec{p}_m S(E_m, \vec{p}_m)}{\int\limits_D dE_m d^3\vec{p}_m S_{PWIA}(E_m, \vec{p}_m)} \,. \tag{2}$$

Here $S_{PWIA}(E_m, \vec{p}_m)$ is the theoretical spectral function of PWIA calculated without taking into account FSI. The missing momentum distribution which is of our interest in the present paper is given by

$$w(\vec{p}_m) = \frac{1}{(2\pi)^3} \int dE_m S(E_m, \vec{p}_m) \,. \tag{3}$$

The distorted spectral function can be written as

$$S(E_m, \vec{p}_m) = \sum_f |M_f(\vec{p}_m)|^2 \delta(E_m + E_{A-1}(\vec{p}_m) + m_p - m_A) \,, \tag{4}$$

where $M_f(\vec{p}_m)$ is the reduced matrix element of the exclusive process $e + A_i \rightarrow e' + (A-1)_f + p$. Then, the missing momentum distribution reads

$$w(\vec{p}_m) = \frac{1}{(2\pi)^3} \sum_f |M_f(\vec{p}_m)|^2 \,. \tag{5}$$

In our analysis we confine ourselves to a large mass number of the target nucleus $A \gg 1$. Then, neglecting the center of mass correlations we can write $M_f(\vec{p}_m)$ as

$$M_f(\vec{p}_m) = \int d^3\vec{r}_1 ... d^3\vec{r}_A \Psi_f^*(\vec{r}_2, ..., \vec{r}_A) \Psi_i(\vec{r}_1, ..., \vec{r}_A) S(\vec{r}_1, ...\vec{r}_A) \exp(i\vec{p}_m\vec{r}_1) \,. \tag{6}$$

Here Ψ_i and Ψ_f are wave functions of the target and residual nucleus, respectively. The nucleon "1" is chosen to be the struck proton. For the sake of brevity, in Eq (6) and hereafter the spin and isospin variables are suppressed. The factor $S(\vec{r}_1, ..., \vec{r}_A)$, which takes into account FSI of the ejectile state with spectator nucleons, is given by

$$S(\vec{r}_1, \vec{r}_2, ..., \vec{r}_A) = \frac{\langle p|\hat{S}_{3q}(\vec{r}_1, \vec{r}_2, ..., \vec{r}_A)|E\rangle}{\langle p|E\rangle} \,, \tag{7}$$

where $|E\rangle$ is a three-quark wave function which describes the state of the proton after absorption of the virtual photon at point $\vec{r}_1$ and $\hat{S}_{3q}(\vec{r}_1, \vec{r}_2, ..., \vec{r}_A)$ is an evolution operator of the three-quark system in the nuclear medium (as usual we assume that the spectator coordinates may be considered frozen during propagation of the fast $3q$ system through

the nuclear medium). In the right-hand side of Eq. (7) the numerator is the probability amplitude for the $3q$ ejectile state escaping from the target nucleus $(A-1)_f$ debris to be observed in the proton state $|p\rangle$, and the denominator is the probability amplitude for the state $|E\rangle$ to be observed in the proton state as well. In terms of the electromagnetic current operator $\hat{J}_{em}$, the ejectile wave function is expressed as [9]

$$|E\rangle = \hat{J}_{em}(Q)|p\rangle = \sum_i |i\rangle\langle i|J_{em}(Q)|p\rangle = \sum_i G_{ip}(Q)|i\rangle \,, \tag{8}$$

where $G_{ip}(Q) = \langle i|J_{em}(Q)|p\rangle$ includes the electromagnetic form factor of the proton as well as all the transition form factors for the electroexcitation of the proton $e + p \rightarrow e' + i$. It is worth noting that the ejectile wave function (8) is independent of the missing momentum and $\vec{p}_m$-dependence of the reduced matrix element emerges only through the exponential $\exp(i\vec{p}_m\vec{r}_1)$ in the right-hand side of Eq. (6).

In the coupled-channel formalism the evolution operator of the $3q$ system can be written in the following form

$$\hat{S}_{3q}(\vec{r}_1, ..., \vec{r}_A) = \hat{P}_z \prod_{j=2}^{A} \left[1 - \theta(z_j - z_1)\hat{\Gamma}(\vec{b}_j - \vec{b}_1, z_j - z_1)\right] \,, \tag{9}$$

where $\vec{b}_j$ and z_j are the transverse and longitudinal coordinates of the nucleons, $\hat{\Gamma}(\vec{b}, z)$ is the operator profile function describing $3q$-nucleon scattering. At high energy the $3q$ system propagates along the straight-path trajectory and can interact with the spectator nucleon "j" only provided that $z_j > z_1$, which is an origin of the z-ordering operator $\hat{P}_z$ and of the step-function $\theta(z_j - z_1)$ in Eq. (9). The matrix elements of the z-dependent operator profile function $\hat{\Gamma}(\vec{b}, z)$ can be written as

$$\langle i|\hat{\Gamma}(\vec{b}, z)|j\rangle = \exp(ik_{ij}z)\langle i|\hat{\Gamma}(\vec{b})|j\rangle \,, \tag{10}$$

where $\hat{\Gamma}(\vec{b})$ is the usual operator profile function connected with the scattering matrix, $\hat{f}$, through the relation

$$\langle i|\hat{\Gamma}(\vec{b})|j\rangle = -\frac{i}{8\pi^2}\int d^2\vec{q}\exp(i\vec{q}\vec{b})\langle i|\hat{f}(\vec{q})|j\rangle \tag{11}$$

(the normalization of the scattering matrix is such that $\mathrm{Im}\langle i|\hat{f}(\vec{q}=0)|i\rangle = \sigma_{tot}(iN))$, and k_{ij} is the longitudinal momentum transfer related to transition $iN \to jN$ [5]

$$k_{ij} = \frac{m_i^2 - m_j^2}{2\varepsilon}\,, \tag{12}$$

here ε is the energy of the struck proton in the laboratory frame, m_i and m_j are the masses of the states $|i\rangle$ and $|j\rangle$. The exponential phase factor in Eq. (10) results from the additional phase which the $3q$ plane wave acquires after propagating the distance z. The whole phase factor, which the operator (9) yields in the case of the sequence of intermediate states $i_1 \to ... \to i_\nu \to p$, is given by

$$F(i_1 \to ... \to i_\nu \to p) = \exp\left[i\sum_{j=1}^{\nu} k_{pi_j}(z_j - z_{j-1})\right]\,, \tag{13}$$

where z_j $(j \geq 1)$ is the longitudinal coordinate of the point where the transition $i_jN \to i_{j+1}N$ takes place, and z_0 corresponds to the transition $p + \gamma^* \to i_1$. It is easy to check, that the same phase factor (13) can be obtained by solving the set of the coupled-channel wave equations.

The sum over the final states of the residual nucleus in Eq. (5) can be performed with the help of the closure relation

$$\sum_f \Psi_f(\vec{r}_2^{\,'}, ..., \vec{r}_A^{\,'})\Psi_f^*(\vec{r}_2, ..., \vec{r}_A) = \prod_{j=2}^{A}\delta(\vec{r}_j - \vec{r}_j^{\,'})\,. \tag{14}$$

After making use of (6), (14), the missing momentum distribution (5) can be cast in the form

$$w(\vec{p}_m) = \frac{1}{(2\pi)^3}\int d^3\vec{r}_1 d^3\vec{r}_1^{\,'}\rho_D(\vec{r}_1, \vec{r}_1^{\,'})\exp[i\vec{p}_m(\vec{r}_1 - \vec{r}_1^{\,'})]\,, \tag{15}$$

where

$$\rho_D(\vec{r}_1, \vec{r}_1^{\,'}) = \int\prod_{j=2}^{A} d^3\vec{r}_j\Psi_i(\vec{r}_1, \vec{r}_2, ..., \vec{r}_A)\Psi_i^*(\vec{r}_1^{\,'}, \vec{r}_2, ..., \vec{r}_A)S(\vec{r}_1, \vec{r}_2, ..., \vec{r}_A)S^*(\vec{r}_1^{\,'}, \vec{r}_2, ..., \vec{r}_A)\,. \tag{16}$$

The function $\rho_D(\vec{r}_1, \vec{r}_1^{\,'})$ can be viewed as a FSI-modified one-body proton density matrix. In PWIA, when the FSI factors in the right-hand side of Eq. (16) equal unity, (16) reduces

to the formula for usual one-body proton density matrix $\rho(\vec{r}_1, \vec{r}_1^{\,'})$, and Eq. (15) reduces to the expression for SPMD

$$n_F(\vec{p}_m) = \frac{1}{(2\pi)^3} \int d\vec{r}_1 d\vec{r}_1^{\,'} \rho(\vec{r}_1, \vec{r}_1^{\,'}) \exp\left[i\vec{p}_m(\vec{r}_1 - \vec{r}_1^{\,'})\right] . \tag{17}$$

As was stated in section 1, we will describe the target nucleus in the independent particle shell model. After neglecting the SRC the A-body semidiagonal density matrix $\Psi_i(\vec{r}_1, \vec{r}_2, ..., \vec{r}_A)\Psi_i^*(\vec{r}_1^{\,'}, \vec{r}_2, ..., \vec{r}_A)$ in Eq. (16) still contains the Fermi correlations. To carry out the integration over the coordinates of the spectator nucleons we neglect the Fermi correlations and replace the A-body semidiagonal density matrix by the factorized form

$$\Psi_i(\vec{r}_1, \vec{r}_2, ..., \vec{r}_A)\Psi_i^*(\vec{r}_1^{\,'}, \vec{r}_2, ..., \vec{r}_A) \to \rho(\vec{r}_1, \vec{r}_1^{\,'}) \prod_{i=2}^{A} \rho(\vec{r}_i) . \tag{18}$$

Here

$$\rho(\vec{r}_1, \vec{r}_1^{\,'}) = \frac{1}{Z} \sum_n \phi_n^*(\vec{r}_1^{\,'}) \phi_n(\vec{r}_1)$$

is the proton shell model one-body density matrix and ϕ_n are the shell model wave functions, $\rho_A(\vec{r})$ is the normalized to unity nucleon nuclear density. The errors connected with ignoring the Fermi correlations must be small because the ratio between the Fermi correlation length $l_F \sim 3/k_F$ and the interaction length corresponding to the interaction of the struck proton with the Fermi correlated spectator nucleons $l_{int} \sim 4(\sigma_{tot}(pN)\langle n_A \rangle)^{-1}$ (here $\langle n_A \rangle$ is the average nucleon nuclear density) is a small quantity (~ 0.25). Recall that the factored approximation for the many-body nuclear density has been successfully employed, in connection with Glauber theory, in the analysis of a wealth of hadron-nucleus scattering data (for an extensive review on hA scattering see [26]).

Making use of replacement (18) in Eq. (16) allows to write the missing momentum distribution in the form

$$w(\vec{p}_m) = \frac{1}{(2\pi)^3} \int d^3\vec{r}_1 d^3\vec{r}_1^{\,'} \rho(\vec{r}_1, \vec{r}_1^{\,'}) \Phi(\vec{r}_1, \vec{r}_1^{\,'}) \exp[i\vec{p}_m(\vec{r}_1 - \vec{r}_1^{\,'})] , \tag{19}$$

where the FSI factor $\Phi(\vec{r}_1, \vec{r}_1^{\,'})$ is given by

$$\Phi(\vec{r}_1,\vec{r}_1^{\,'}) = \int \prod_{j=2}^{A} \rho_A(\vec{r}_j) d^3\vec{r}_j S(\vec{r}_1,\vec{r}_2,...,\vec{r}_A) S^*(\vec{r}_1^{\,'},\vec{r}_2,...,\vec{r}_A)\,. \tag{20}$$

Substituting (7) into (20) we may write the FSI factor $\Phi(\vec{r}_1,\vec{r}_1^{\,'})$ in the following operator form

$$\Phi(\vec{r}_1,\vec{r}_1^{\,'}) = \langle pp|\hat{U}(\vec{r}_1,\vec{r}_1^{\,'})|ii^{'}\rangle C_i C^*_{i'}\ , \tag{21}$$

where

$$C_i = \frac{\langle i|E\rangle}{\langle p|E\rangle}\,,$$

and the operator $\hat{U}(\vec{r}_1,\vec{r}_1^{\,'})$ is an evolution operator for the density matrix of the $3q$ system in the nuclear medium

$$\hat{U}(\vec{r}_1,\vec{r}_1^{\,'}) = \int \prod_{j=2}^{A} \rho_A(\vec{r}_j) d^3\vec{r}_j \hat{S}_{3q}(\vec{r}_1,\vec{r}_2,...,\vec{r}_A) \hat{S}^*_{3q}(\vec{r}_1^{\,'},\vec{r}_2,...,\vec{r}_A)\,. \tag{22}$$

After substitution of the CCMST expression (9) for $\hat{S}_{3q}$ into Eq. (22) it takes the form

$$\begin{aligned}\hat{U}(\vec{r}_1,\vec{r}_1^{\,'}) = \hat{P}_z \Bigg[1 &- \int\limits_{z_1}^{\infty} dz \int d^2\vec{b}\,\hat{\Gamma}(\vec{b}-\vec{b}_1, z-z_1)\rho_A(\vec{b},z) \\ &- \int\limits_{z_1^{'}}^{\infty} dz \int d^2\vec{b}\,\hat{\Gamma}^*(\vec{b}-\vec{b}_1^{\,'}, z-z_1^{'})\rho_A(\vec{b},z) \\ &+ \int\limits_{max(z_1,z_1^{'})}^{\infty} dz \int d^2\vec{b}\,\hat{\Gamma}(\vec{b}-\vec{b}_1, z-z_1)\hat{\Gamma}^*(\vec{b}-\vec{b}_1^{\,'}, z-z_1^{'})\rho_A(\vec{b},z) \Bigg]^{A-1}\,. \end{aligned} \tag{23}$$

We will refer to the first two terms in the square brackets in the right-hand side of (23) as $\hat{\Gamma}(\hat{\Gamma}^*)$ terms, and to the last one as $\hat{\Gamma}\hat{\Gamma}^*$ term. The operator (23) can be graphically represented by the sum of the diagrams as shown in Fig. 1. Every dotted line attached to the straight-line trajectory originating from the point $\vec{r}_1$ ($\vec{r}_1^{\,'}$) denotes a profile function $\hat{\Gamma}(\vec{b}_j-\vec{b}_1, z_j-z_1)$ ($\hat{\Gamma}^*(\vec{b}_j-\vec{b}_1^{\,'}, z_j-z_1^{'})$). The interaction between the two trajectories generated by the diagrams like shown in Fig. 1b does not allow one to represent (23) in a factorized form in coordinate and internal space of the two $3q$ systems propagating along the trajectories originating from $\vec{r}_1$ and $\vec{r}_1^{\,'}$.

The emergence of the evolution operator for the $3q$ density matrix in Eq. (21) is not surprising since we evaluate the probability distribution for a subsystem (the $3q$ ejectile state) in the process involving a complex system (the $3q$ ejectile state and the residual nucleus). It is worth recalling that similar interaction between the trajectories emerges also in the related problem of passage of the ultrarelativistic positronium through matter [27].

Eq. (23) can further be simplified exploiting the fact that $\rho_A(\vec{b},z)$ is a smooth function of the impact parameter $\vec{b}$ as compared to the operator profile function. In leading order in the small parameter R^2_{3qN}/R^2_A (R_{3qN} is a radius of $3q$-nucleon interaction and R_A is the nucleus radius) we have

$$\int d^2\vec{b}\,\hat{\Gamma}(\vec{b}-\vec{b}_1,z-z_1)\rho_A(\vec{b},z) \approx \frac{\hat{\sigma}(z)}{2}\rho_A(\vec{b},z)\,, \tag{24}$$

$$\int d^2\vec{b}\,\hat{\Gamma}(\vec{b}-\vec{b}_1,z-z_1)\hat{\Gamma}^*(\vec{b}-\vec{b}_1^{\,\prime},z-z_1^{\,\prime})\rho_A(\vec{b},z) \approx \hat{\eta}(\vec{b}_1-\vec{b}_1^{\,\prime},z-z_1,z-z_1^{\,\prime})\rho_A(\frac{1}{2}(\vec{b}_1+\vec{b}_1^{\,\prime}),z)\ , \tag{25}$$

where

$$\hat{\sigma}(z) = 2\int d^2\vec{b}\,\hat{\Gamma}(\vec{b},z)\,, \tag{26}$$

$$\hat{\eta}(\vec{b},z,z') = \int d^2\vec{\Delta}\hat{\Gamma}(\vec{b}-\vec{\Delta},z)\hat{\Gamma}^*(\vec{\Delta},z')\,. \tag{27}$$

In terms of the diffraction scattering matrix $\hat{f}$ the matrix elements of the z-dependent operators (26), (27) are given by

$$\langle i|\hat{\sigma}(z)|k\rangle = -i\exp(ik_{ij}z)\langle i|\hat{f}(\vec{q}=0)|k\rangle\,, \tag{28}$$

$$\langle ii'|\hat{\eta}(\vec{b},z,z')|kk'\rangle = \frac{\exp[i(k_{ik}z-k_{i'k'}z')]}{16\pi^2}\int d^2\vec{q}\exp(i\vec{q}\vec{b})\langle i|\hat{f}(\vec{q})|k\rangle\langle i'|\hat{f}(-\vec{q})|k'\rangle^*\,. \tag{29}$$

The results of the analysis of $(e,e'p)$ scattering within the Glauber model [17] indicate that the variations of the missing momentum distribution connected with the smearing corrections to the approximations (24), (25) are $\lesssim 3\%$ at $p_m \lesssim 300$ MeV/c.

Making use of Eqs. (23)-(25) and exponentiating which is a good approximation at $A \gtrsim 10$ we finally get

$$\hat{U}(\vec{r}_1, \vec{r}_1^{\,\prime}) = \hat{P}_z \exp\left[-\frac{1}{2} \int\limits_{z_1}^{\infty} dz\, \hat{\sigma}(z - z_1) n_A(\vec{b}_1, z) - \frac{1}{2} \int\limits_{z_1^{\prime}}^{\infty} dz\, \hat{\sigma}^*(z - z_1^{\prime}) n_A(\vec{b}_1^{\,\prime}, z) \right.$$
$$\left. + \int\limits_{max(z_1, z_1^{\prime})}^{\infty} dz\, \hat{\eta}(\vec{b}_1 - \vec{b}_1^{\,\prime}, z - z_1, z - z_1^{\prime}) n_A(\frac{1}{2}(\vec{b}_1 + \vec{b}_1^{\,\prime}), z) \right] , \tag{30}$$

where $n_A(\vec{r}) = A\rho_A(\vec{r})$ is the nucleon nuclear density.

As one can see from Eq. (27) the $\hat{\Gamma}\hat{\Gamma}^*$ term in Eqs. (23), (30) becomes only important when $|\vec{b}_1 - \vec{b}_1^{\,\prime}| \lesssim R_{3qN} \sim 1$ fm. Such a short range interaction between the two trajectories in the impact parameter plane must for the most part affect the missing momentum distribution at $p_m \gtrsim 1/R_{3qN} \sim 200$ MeV/c. This fact becomes evident if one rewrites Eq. (19) in the convolution form

$$w(\vec{p}_m) = \frac{1}{(2\pi)^6} \int d^3\vec{R} \int d^3\vec{k} W_\rho(\vec{R}, \vec{p}_m - \vec{k}) W_\Phi(\vec{R}, \vec{k}) \, , \tag{31}$$

where

$$W_\rho(\vec{R}, \vec{k}) = \int d^3\vec{r} \rho(\vec{R} + \vec{r}/2, \vec{R} - \vec{r}/2) \exp(i\vec{k}\vec{r}) \tag{32}$$

is the familiar Wigner function, and

$$W_\Phi(\vec{R}, \vec{k}) = \int d^3\vec{r} \Phi(\vec{R} + \vec{r}/2, \vec{R} - \vec{r}/2) \exp(i\vec{k}\vec{r}) \, . \tag{33}$$

The representation (31) makes it clear that the short range interaction between the two trajectories generated by the $\hat{\Gamma}\hat{\Gamma}^*$ term, which converts after Fourier transform (33) into the slowly decreasing tails of $W_\Phi(\vec{R}, \vec{k})$, will reveal itself for the most part at large missing momenta. Remarkably, although the operator $\hat{\eta}(\vec{b}, z, z')$ defined by Eq. (27) has the short range behavior only in the impact parameter plane, the $\hat{\Gamma}\hat{\Gamma}^*$ term in Eq. (30) generates the slow decreasing tails of $W_\Phi(\vec{R}, \vec{k})$ in the longitudinal momenta as well. A formal origin of this effect is the non-analytical behavior at $z_1 = z_1^{\prime}$ of the function $max(z_1, z_1^{\prime}) = (z_1 + z_1^{\prime} +$

$|z_1 - z_1^{'}|)/2$, which is the low limit of integration over z in the $\hat{\Gamma}\hat{\Gamma}^*$ term in Eq. (30). Such a non-analytical function derives from the absence of an incoming proton plane wave, which is a real physical reason for affecting the longitudinal missing momentum distribution by the $\hat{\Gamma}\hat{\Gamma}^*$ term (for the detailed quantum mechanical analysis of this phenomenon see ref. [17]).

In the Glauber analysis of $(e, e'p)$ scattering [17] it was shown that the $\hat{\Gamma}\hat{\Gamma}^*$-generated effects correspond to the incoherent rescatterings of the struck proton in the nuclear medium, while the $\hat{\Gamma}(\hat{\Gamma}^*)$ terms describe FSI related to the coherent rescatterings. ¿From the point of view of the shell model the theoretical predictions obtained without taking into account the $\hat{\Gamma}\hat{\Gamma}^*$ term correspond to the exclusive $(e, e'p)$ scattering, when only the one-hole excitations of the target nucleus are allowed , while the whole FSI factor including the $\hat{\Gamma}\hat{\Gamma}^*$ term corresponds to the inclusive process, when all the final states of the residual nucleus are included [17]. The results of ref. [17] show that the $\hat{\Gamma}\hat{\Gamma}^*$ term increases the missing momentum distribution by 3-7% at $|\vec{p}_m| \lesssim 250$ MeV/c in the parallel kinematics. For the transverse kinematics the same estimate is valid for $p_{m\perp} \lesssim 200$ MeV/c. The $\hat{\Gamma}\hat{\Gamma}^*$ term becomes especially important in the region of $p_{m\perp} \gtrsim 250$ MeV/c, where it dominates in the missing momentum distribution. Evidently, approximately the same situation will take place in CCMST in the regime of the onset of CT.

The theoretical study of CT effects including the $\hat{\Gamma}\hat{\Gamma}^*$ term in the region of large transverse missing momenta would be of great interest because in this case the missing momentum distribution probes the $3q$-nucleon scattering amplitude when the $3q$ wave function is still close to the initial ejectile wave function. Unfortunately, the calculations including the $\hat{\Gamma}\hat{\Gamma}^*$ term require the information about $3q$-nucleon diffraction scattering matrix at arbitrary momentum transfer, as one can see from Eq. (29). It renders difficult an accurate estimate of the CT effects for the inclusive $(e, e'p)$ reaction in the region of large p_m. Still, even a qualitative understanding of the role of the $\hat{\Gamma}\hat{\Gamma}^*$ term is interesting and we comment on that in section 4. We postpone a detail analysis of the inclusive

reaction at large p_m for further publications.

In the present paper we focus on the numerical calculations of the missing momentum distribution for exclusive $(e, e'p)$ reaction, when the FSI is exhausted by the coherent rescatterings. The corresponding FSI factor (we label it as Φ_{coh}), which may be obtained from Eq. (20) after neglecting the $\hat{\Gamma}\hat{\Gamma}^*$ term in the evolution operator (30), has the following factorized form

$$\Phi_{coh}(\vec{r}_1, \vec{r}_1^{\,'}) = S_{coh}(\vec{r}_1) S_{coh}(\vec{r}_1^{\,'})^* \tag{34}$$

where

$$S_{coh}(\vec{r}_1) = \langle p|\hat{P}_z \exp\left[-\frac{1}{2}\int\limits_{z_1}^{\infty} dz \hat{\sigma}(z-z_1) n_A(\vec{b}_1, z)\right] |i\rangle C_i \ . \tag{35}$$

Substituting (34) into (19) we arrive at the following expression for the missing momentum distribution

$$w(\vec{p}_m) = \frac{1}{Z}\sum_n \left| \int d^3\vec{r}\, \phi_n(\vec{r}) \exp(i\vec{p}_m\vec{r}) S_{coh}(\vec{r}) \right|^2 \ . \tag{36}$$

Eq. (36) can be also obtained directly from Eqs. (5), (6) if one includes in the sum over the final states of the residual nucleus in Eq. (5) only the one-hole excitations and neglects the Fermi correlations between the spectator nucleons. For the related intuitive optical potential consideration see refs. [7,8,10].

¿From the point of view of numerical calculations it is convenient to evaluate $S_{coh}(\vec{r})$ treating in Eq. (35) the nondiagonal part of matrix $\hat{\sigma}(z-z_1)$ as a perturbation. Then, the FSI factor (35) can be expanded in the ν-fold off-diagonal rescatterings series

$$S_{coh}(\vec{r}) = \sum_{\nu=0}^{\infty} S_{coh}^{(\nu)}(\vec{r}) \,, \tag{37}$$

where

$$S_{coh}^{(0)}(\vec{r}) = \exp[-\frac{1}{2} t(\vec{b}, \infty, z)\sigma_{pp}] \,, \tag{38}$$

and

$$S^{(\nu)}_{coh}(\vec{b},z)=\left(-\frac{1}{2}\right)^{\nu}\sum_{i_1,...i_\nu}\sigma^{'}_{pi_\nu}\sigma^{'}_{i_\nu i_{\nu-1}}\cdots\sigma^{'}_{i_2 i_1}\frac{\langle i_1|E\rangle}{\langle p|E\rangle}\exp[ik_{i_1 p}z]\int\limits_{z}^{\infty}dz_1 n_A(\vec{b},z_1)$$

$$\times\exp[ik_{i_2 i_1}z_1-\frac{1}{2}t(\vec{b},z_1,z)\sigma_{i_1 i_1}]\int\limits_{z_1}^{\infty}dz_2 n_A(\vec{b},z_2)\exp[ik_{i_3 i_2}z_2-\frac{1}{2}t(\vec{b},z_2,z_1)\sigma_{i_2 i_2}]\cdots$$

$$\times\int\limits_{z_{\nu-1}}^{\infty}dz_\nu n_A(\vec{b},z_\nu)\exp[ik_{pi_\nu}z_\nu-\frac{1}{2}t(\vec{b},\infty,z_\nu)\sigma_{pp}]\,,\qquad\nu\geq 1\,. \quad (39)$$

Here $\vec{r}=(\vec{b},z)$, $\sigma^{'}_{ik}=\sigma_{ik}-\delta_{ik}\sigma_{ii}$, the matrix $\hat{\sigma}$ is connected with the forward diffraction scattering matrix $\hat{f}(\vec{q}=0)=i\hat{\sigma}$ and $t(\vec{b},z_2,z_1)=\int_{z_1}^{z_2}dz n_A(\vec{b},z)$ is the partial optical thickness. The zeroth order term $S^{(0)}(\vec{r})$ in Eq. (37) describes the conventional Glauber result, while the terms with $\nu\geq 1$ correspond to the inelastic intermediate states contributing to electroexcitation and diffractive de-excitation of the proton $p\to i_1\to ...\to i_\nu\to p$. It is precisely the oscillating exponential phase factors in Eq. (39), which leads to suppression of the contributions of the inelastic intermediate states at low energies of the struck proton. They are also the origin of the longitudinal asymmetry of the nuclear transparency produced by the off-diagonal rescatterings. The emergence of these oscillating factors is a purely quantum mechanical effect. In the classical treatment of FSI in terms of z-dependent $3q$-nucleon cross section of ref. [22] it is lacking and the longitudinal asymmetry of the missing momentum distribution vanishes.

Eqs. (36)-(39) form a basis for evaluation of the missing momentum distribution within CCMST for the exclusive $(e,e'p)$ reaction. In the region of $p_m\lesssim 150-200$ MeV/c, where the effect of the incoherent rescatterings becomes small, our predictions can be compared directly with experimental data obtained without restrictions on the final states of the residual nucleus.

III. PARAMETERIZATION OF THE DIFFRACTION MATRIX AND THE INITIAL EJECTILE WAVE FUNCTION

To proceed further with the numerical calculation of nuclear transparency we need the diffraction matrix describing $3q$-nucleon scattering and initial ejectile wave function. At GeV's energies of the struck proton, which are of our interest in the present paper, the major contribution to the imaginary part of the amplitude $f(kN \to iN)$ comes from the Pomeron exchange. Namely this component of the $3q$-nucleon scattering matrix is for the most part important from the point of view of CT. Following ref. [6] we construct the Pomeron component of $\hat{\sigma}$ using the oscillator quark-diquark model of the proton:

$$\text{Im } f_P(kN \to iN) = \text{Re } \sigma_{ik}^P = \int dz d^2\vec{\rho}\, \Psi_i^*(\vec{\rho}, z)\sigma(\rho)\Psi_k(\vec{\rho}, z)\,, \tag{40}$$

where $\Psi_{i,k}(\vec{\rho}, z)$ are the oscillator wave functions describing the quark-diquark states and $\sigma(\rho)$ is the dipole cross section describing the interaction of the quark-diquark system with a nucleon. For the oscillator frequency of the quark-diquark system we use the value $\omega_{qD} = 0.35$ GeV, leading to a realistic mass spectrum of the proton excitations. As in ref. [6] we take the dipole cross section in the form

$$\sigma(\rho) = \sigma_0 \left[1 - \exp\left(-\frac{\rho^2}{R_0^2}\right)\right]\,. \tag{41}$$

Eq. (41) is motivated by the results of the calculation of the $q\bar{q}$ dipole cross section in the double gluon exchange model of the Pomeron [28]. The parameterization (41) with $\sigma_0 \approx 50-60$ mb and $R_0 \approx 1.2-1.4$ fm allows one to describe both the CT effects in quasielastic charge exchange reaction $\pi^- A \to \pi^o A'$ [29] and the nuclear shadowing and diffraction cross section in deep inelastic scattering [30,31]. The $q\bar{q}$ dipole cross section extracted from the experimental data on the vector meson electroproduction [32] also appears to be close to the one used in refs. [29–31]. Of course, due to the nonzero diquark size, the parameters of the quark-diquark dipole cross section in Eq. (41) may differ from the ones obtained from the analysis of meson exchange process and deep inelastic scattering. Following ref.

[6], we set $\sigma_0 = 80$ mb and adjust R_0 to reproduce $\sigma_{tot}^{exp}(pN)$. ¿From the point of view of realistic evaluation of the onset of CT it is important for the model diffraction matrix to reproduce the gross features of diffractive pN scattering in the resonance region. Our diffraction matrix obtained with the above set of parameters yields the value of the ratio between the diffractive and elastic pN cross sections $\sigma_{diff}(pp)/\sigma_{el}(pp) \approx 0.25$, which is in agreement with the experimental data [33]. Moreover, we obtain a good description of the diffractive mass spectrum observed in pN scattering [34].

The real parts of the diagonal $f(iN \to iN)$, for $i \neq p$, and off-diagonal $f(iN \to kN)$ amplitudes are not known experimentally. At GeV's energy of the struck proton they are connected with the reggeon exchanges. In the counterdistinction to the Pomeron exchange we do not have at present a reliable theoretical model for the reggeon contribution to the $3q$-nucleon amplitudes even for a small-size $3q$ system. As a reference value, we consider the choice $\alpha_1 = 1$, $\alpha_2 = 0$ in the parameterizations

$$\begin{aligned} \text{Re } f_R(iN \to iN) = \alpha_1 \text{Re } f_R(pN \to pN) = \frac{\alpha_1}{2} \left(\alpha_{pp}\sigma_{tot}(pp) + \alpha_{pn}\sigma_{tot}(pn)\right) , \\ \text{Re } f_R(iN \to kN) = \alpha_2 \text{Im } f_P(iN \to kN) , \quad i \neq k . \end{aligned} \tag{42}$$

Even though the above choice of $\alpha_{1,2}$ can be justified within the framework of the dual parton model [35] we are fully aware that it should only be regarded as an estimate, and will study the sensitivity of the results to the values of $\alpha_{1,2}$.

Besides the matrix $\hat{\sigma}$, the evaluation of $w(\vec{p}_m)$ requires the initial ejectile wave function $|E\rangle$. In the present paper we optimize for CT effects, assuming the dominance of the small-size $3q$ configurations in the matrix elements $\langle i|J_{em}(Q)|p\rangle$ for the resonance states with masses in the GeV's region [1]. This amounts to a strong assumption that the probability amplitude for the initial ejectile state to be observed in state $|i\rangle$,

$$\langle i|E\rangle = \langle i|J_{em}(Q)|p\rangle \propto \phi_i^*(\rho \sim \frac{1}{Q}) , \tag{43}$$

where ϕ_i is the coordinate wave function of the state $|i\rangle$. By virtue of Eq. (43) the initial ejectile wave function can be chosen in a point-like form. We parametrize it in the form

$\langle\rho|E\rangle \propto \exp(-C\rho^2Q^2)$, with $C = 1$. We would like to emphasize that the possibility of using the point-like initial ejectile wave function for the study of CT effects by no means implies that the real ejectile state $|E\rangle$ actually has a size $\sim 1/Q$. On the contrary, it is evident that the ejectile state formed after absorption of the virtual photon has exactly the same transverse size as the proton [36]. The solution to this puzzling situation is obvious. Eq. (43) is only valid for electroproduction of the proton and its low-mass excitations, which requires the hard gluon exchanges between the quarks of the $3q$ system. The electroproduction of the high mass states with masses $\sim |\vec{q}|$ does not require such exchanges, and Eq. (43) does not hold in this case. However, the off-diagonal rescatterings including the heavy intermediate states are suppressed. First, due to the oscillating factors in Eq. (39) only the states which satisfy the coherency constraint $m^{*^2} - m_p^2 \lesssim Q^2/R_A m_p$ can contribute to FSI. Second, the off-diagonal diffraction amplitudes $f(iN \to jN)$ also become small when the masses m_i and m_j differ strongly.

The above suppression of the heavy intermediate states makes the theoretical predictions insensitive to the specific form of the point-like initial ejectile wave function. For instance, for Gaussian parameterization used in the present paper the missing momentum distribution must be insensitive to the value of C as long as $C \gtrsim 1/Q^2\rho_o^2$, where ρ_o denotes the position of the first node in the wave functions of the excited states satisfying the coherency requirement. We checked that in the region of $Q^2 \lesssim 40$ GeV^2, which we discuss in the present paper, our numerical results are practically independent of the parameter C for $C \gtrsim 0.1$. It is worth noting that the weak sensitivity of CT effects to the specific choice of the point-like initial ejectile wave function also vindicates neglecting the difference between the CT effects for the longitudinal and transverse spectral functions.

In conclusion of this section one remark on the nonrelativistic description of the $3q$ system is in order. Of course, the nonrelativistic approach can not be justified for the high excited states. However, our numerical results show that due to the coherency constraint the dominant role in the regime of the onset of CT plays the first excitation

of the proton. This, in part, vindicates the use of the nonrelativistic model. Still, we regard the nonrelativistic quark-diquark model only as a basis which allows us to obtain a realistic diffraction scattering matrix, which is truly important from the point of view of CCMST.

IV. QUALITATIVE ANALYSIS OF THE INCOHERENT FSI

As was shown in section 2 an evaluation of the missing momentum distribution with the $\hat{\Gamma}\hat{\Gamma}^*$ term included requires the information on the $3q$-nucleon scattering matrix at arbitrary momentum transfer. Despite the ensuing model-dependence of an analysis of the inclusive $(e, e'p)$ reaction, certain conclusions on the role of the incoherent rescatterings can be reached without specifying the explicit form of the scattering matrix. Here we consider the simpler case of the integrated nuclear transparency. For the case of the inclusive $(e, e'p)$ reaction we can write

$$T_A^{inc} = T_A^{exc} + \Delta T_A \,, \tag{44}$$

where

$$T_A^{exc} = \int d^3\vec{r}\rho_A(\vec{r})\Phi_{coh}(\vec{r},\vec{r}\,) \,, \tag{45}$$

is the transparency for exclusive $(e, e'p)$ scattering when only the coherent rescatterings are allowed, and the contribution of the incoherent FSI is given by

$$\Delta T_A = \int d^3\vec{r}\rho_A(\vec{r})[\Phi(\vec{r},\vec{r}\,) - \Phi_{coh}(\vec{r},\vec{r}\,)] \,. \tag{46}$$

To simplify the problem let us consider the two-channel model, which involves only one resonance state $|p^*\rangle$. We estimate ΔT_A expanding the evolution operator (30) up to first order in the $\hat{\Gamma}\hat{\Gamma}^*$ term. Notice that the one-fold incoherent rescattering practically saturates the missing momentum distribution in the region of $p_m \lesssim 300$ MeV/c, which gives the dominant contribution to T_A^{inc} [17]. Also, we neglect the off-diagonal coherent

rescatterings. Then, making use of Eqs. (21), (30), (34), (46) after some simple algebra we get

$$\Delta T_A = \frac{1}{16\pi^2}\int d^2\vec{q}\Big[|\langle p|\hat{f}(\vec{q})|p\rangle|^2 I_{pp} + |\langle p|\hat{f}(\vec{q})|p^*\rangle|^2 I_{p^*p^*}|C_{p^*}|^2 + 2\mathrm{Re}\langle p|\hat{f}(\vec{q})|p^*\rangle\langle p|\hat{f}(\vec{q})|p\rangle^* I_{p^*p}C_{p^*}\Big]\,. \tag{47}$$

Here

$$I_{pp} = \int d^2\vec{b}_1 dz_1 \rho_A(\vec{b}_1, z_1)\int\limits_{z_1}^{\infty} dz\, n_A(\vec{b}_1, z)\exp\Big[-\mathrm{Re}\sigma_{pp}t(\vec{b}_1,\infty,z_1)\Big]\,, \tag{48}$$

$$I_{p^*p^*} = \int d^2\vec{b}_1 dz_1 \rho_A(\vec{b}_1, z_1)\int\limits_{z_1}^{\infty} dz n_A(\vec{b}_1, z) \times\exp\Big[-\mathrm{Re}\sigma_{pp}t(\vec{b}_1,\infty,z) - \mathrm{Re}\sigma_{p^*p^*}t(\vec{b}_1, z, z_1)\Big]\,, \tag{49}$$

$$I_{p^*p} = \int d^2\vec{b}_1 dz_1 \rho_A(\vec{b}_1, z_1)\int\limits_{z_1}^{\infty} dz\, n_A(\vec{b}_1, z)\exp(ik_{pp^*}z) \times\exp\left[-\mathrm{Re}\sigma_{pp}t(\vec{b}_1,\infty,z) - \frac{(\sigma_{p^*p^*}+\sigma^*_{pp})}{2}t(\vec{b}_1, z, z_1)\right]\,. \tag{50}$$

The diagonal and off-diagonal amplitudes in Eq. (47) are related through the CT sum rule

$$\langle p|\hat{f}(\vec{q})|p\rangle + \langle p|\hat{f}(\vec{q})|p^*\rangle C_{p^*} = 0\,. \tag{51}$$

Making use of (51) we can write (47) as

$$\Delta T_A = \sigma_{el}(pN)\left[I_{pp} + I_{p^*p^*} - 2\mathrm{Re}I_{p^*p}\right]\,. \tag{52}$$

At low energy of the struck proton, when $k_{pp^*}R_A \approx (m^2_{p^*} - m^2_p)R_A/2\varepsilon \gg 1$, the p^*p interference term in Eq. (52) (the last term in the square brackets in the right hand side of Eq. (52)) becomes small and we get

$$\Delta T_A \approx \sigma_{el}(pN)\left[I_{pp} + I_{p^*p^*}\right]\,. \tag{53}$$

At high energy, when $k_{pp^*}R_A \approx (m^2_{p^*} - m^2_p)R_A/2\varepsilon \ll 1$, the p^*p interference term in Eq. (52) is not suppressed and will in part cancel the contributions of the first two terms. Thus, we see that, on the contrary to the coherent FSI, in the case of the incoherent FSI the CT effects decrease nuclear transparency. Hence, a conspiracy of the CT effects related to the coherent and incoherent rescatterings must take place in the integrated nuclear transparency measured in inclusive $(e, e'p)$ reaction. According to the qualitative consideration of section 2 and the analysis [17], the contribution of the incoherent rescatterings to the missing momentum distribution for the most part comes from the region of $p_{m\perp} \gtrsim 200 - 250$ MeV/c. Evidently, the above discussed difference between ΔT_A at low and high energy comes namely from this region of the missing momentum. Hence, it is advantageous to perform experimental measurements of the nuclear transparency separately in the regions of $p_{m\perp} \lesssim 200$ MeV/c and $p_{m\perp} \gtrsim 250$ MeV/c. At small momenta the CT signal is increasing the transparency, while at large momenta the CT will manifest itself through decreasing the transparency.

Eq. (53) demonstrates that, on the contrary to the wide spread opinion, in inclusive $(e, e'p)$ reaction the contribution of the off-diagonal rescatterings survives at low energies. To this effect, the inclusive $(e, e'p)$ scattering differs drastically from exclusive $(e, e'p)$ reaction or elastic hadron-nucleus scattering, where at low energies the predictions of CCMST and the Glauber model are close to each other. Of course, one should bear in mind that Eq. (53) is obtained in the idealized quark model, which ignores the finite value of the resonance width, Γ_{p^*}. Inclusion of the finite Γ_{p^*} will lead to a suppression of the second term in the right-hand side of Eq. (53) at sufficiently small energies $\varepsilon \lesssim \Gamma_{p^*} m_{p^*} l_{int} \sim 2$ GeV (here $l_{int} \sim (\sigma_{tot}(pN)\langle n_A\rangle)^{-1}$ is the average interaction length of the $3q$ system in the nuclear medium). However, it is important that the scale of the energy , where the finite-width effects become strong, are by the factor $\sim 3-5$ smaller than the energy scale of the CT effects $\varepsilon \sim (m^2_{p^*} - m^2_p)R_A/2$. It means that there is a certain energy interval in which the CT effects are still small but, none the less, the Glauber model is not justified

for evaluation of the contribution to the missing momentum distribution of the incoherent rescatterings.

It is appropriate here to comment on the previous analyses of the Q^2-dependence of the integrated nuclear transparency. In refs. [6–8] the calculations were performed making use of the optical potential form of the FSI factor. It means that the integrated transparency of refs. [6–8] corresponds to the exclusive $(e, e'p)$ reaction. The authors of refs. [11,12] also used the optical potential FSI factor. However, they replaced the total pN cross section by the inelastic pN cross section, $\sigma_{in}(pN)$. In the Glauber model the integrated transparency in the inclusive $(e, e'p)$ scattering is indeed controlled by $\sigma_{in}(pN)$ (see discussion of this problem in [17]). The analysis of the present paper makes clear that the CT effects from the incoherent rescatterings can not be described by a simple renormalization of the diffraction scattering matrix in the equations obtained in the optical potential approach. For this reason prescription of refs. [11,12] is not justified.

It is worth noting that the above analysis indicates that in the case of the quasielastic $(p, 2p)$ scattering also a complicated interplay of the CT effects from the coherent and incoherent rescatterings may take place. Evidently, in this process too the contribution of the off-diagonal incoherent rescatterings will survive at low energies. In $(p, 2p)$ scattering the contribution of the incoherent rescatterings appears to be considerably enhanced in a comparison with $(e, e'p)$ reaction [32]. For this reason an analysis of the CT effects in $(p, 2p)$ scattering must include the incoherent rescatterings, which were neglected in all previous works on this problem.

V. NUMERICAL RESULTS FOR THE EXCLUSIVE $(e, e'p)$ SCATTERING

In this section we present our numerical results for the nuclear transparency in exclusive $(e, e'p)$ scattering obtained making use of Eqs. (36)-(39). We remind, that in the region of $p_m \lesssim 150 - 200$ MeV/c, where the contribution of the incoherent rescatterings becomes small, our theoretical predictions may be compared directly with experimental

data for inclusive $(e, e'p)$ reaction. The numerical calculations were carried out for the target nuclei ^{16}O and ^{40}Ca. We used in our calculations the harmonic oscillator shell wave functions. The oscillator shell model frequency, ω_{osc}, for the two nuclei were adjusted to reproduce the experimental value of the root-mean-square radius of the charge distribution, $\langle r^2\rangle^{1/2}$. We used the values [37] $\langle r^2\rangle^{1/2} = 2.73$ fm for ^{16}O, and $\langle r^2\rangle^{1/2} = 3.47$ fm for ^{40}Ca, which correspond to the oscillator radius, $r_{osc} = (m_p\omega_{osc})^{-1/2}$, equal to 1.74 fm for ^{16}O and 1.95 fm for ^{40}Ca. The difference between the charge distribution and the proton nuclear density connected with the proton charge radius was taken into account. We checked that our set of the harmonic oscillator shell wave functions gives the charge density and SPMD in the region of $p_m \lesssim$(250-300) Mev/c, which are practically indistinguishable from the results of more involved Hartree-Fock calculations. Notice that in this momentum region SPMD calculated in the harmonic oscillator shell model is also close to the one obtained within a many-body approach with realistic nucleon-nucleon potential in ref. [38]. In our calculations we define the pN cross section and α_{pN} as mean values of these quantities for the pp and pn scatterings. We borrowed the experimental data on pp, pn cross sections and α_{pp}, α_{pn} from the recent review [39].

To illustrate the role of the off-diagonal rescatterings, which are responsible for the CT effects, we present a systematic comparison of the results obtained within CCMST and the ones obtained in the Glauber model. The number of the included resonance states and the the multiplicity of the off-diagonal rescatterings used in Eqs. (37)-(39) to obtain the curves corresponding to CCMST were equal to 4 and 3, respectively. We checked that the contributions from higher excitations and rescatterings with $\nu > 3$ are negligible in the region of $Q^2 \lesssim 40$ GeV^2 considered in the present paper.

In Figs. 2, 3 we show the behavior of the nuclear transparency versus $p_{m,z}$ for the purely parallel kinematics at $Q^2 = 5, 10, 20$ and 40 GeV^2. Notice that the nuclear transparency evaluated even in the Glauber model without off-diagonal rescatterings has sizeable asymmetry about $p_{m,z} = 0$ connected with nonzero α_{pN}, which was neglected in

previous works. Figs. 2, 3 demonstrate that the CT effect in the region of $Q^2 \lesssim 10$ GeV^2 is still small at $|p_{m,z}| \lesssim 150$ MeV/c. However, at $p_{m,z} \sim -250$ MeV/c it becomes sizeable and could be observed in a high precision experiment. Our calculations show that the situation is more favorable in the case of light nuclei.

The results for the nuclear transparency for the transverse kinematics are presented in Figs. 4, 5. We see that, as in the case of the parallel kinematics, the distortion effects are considerable even in the Glauber model. The CT effects are still small in the region of $Q^2 \lesssim 10$ GeV^2. They become important only at $Q^2 \gtrsim 20$ GeV^2, especially at large $p_{m\perp}$.

In Figs. 6, 7 we show our predictions for the integrated nuclear transparency. In order to demonstrate the dependence of the nuclear transparency on the choice of the kinematical domain D in the definition (2), we calculated T_A for four different windows in the missing momenta. One sees that the most steep rise of T_A takes place for the window containing negative values of the longitudinal missing momentum.

We also calculated the integrated nuclear transparency for the excitation of separate hole states in the target nucleus for the kinematical domain $p_{m\perp}, |p_{m,z}| < 200$ MeV/c. The results are presented in Figs. 8, 9. These figures show that CT effects are different for the different shell states, being larger for the 1s state. This fact is further illustrated by Figs. 10-13, which show the missing momentum distribution for excitation of the separate hole states for the parallel and transverse kinematics at $Q^2 = 5$ and 40 GeV^2. Unfortunately, however, the experimental information about deeply bound hole states are most difficult to extract, since their strength is fragmented over a wide range missing energy.

The relative CT effect of different excitations of the $3q$ ejectile state is demonstrated in Fig. 10, where we plot the integrated nuclear transparency for the window $p_{m\perp}, |p_{m,z}| <$ 200 MeV/c calculated for the number of included intermediate states, n, equals 1, 2, 3, 4. We see that in the region $Q^2 \lesssim 40$ GeV^2 the FSI effects are practically saturated for $n = 3$. At $Q^2 \lesssim 20$ GeV^2 in the CCMST formalism it is sufficient to take into account

only the first excitation of the proton.

Our numerical results show that the experimental observation of the CT phenomenon at $Q^2 \lesssim 20$ GeV^2 is a delicate problem. For this reason it is important to understand how large are the uncertainties of the theoretical predictions for the contribution of the off-diagonal rescatterings. The least reliable ingredient is the reggeon part of the $3q$-nucleon amplitudes. To estimate the corresponding uncertainties we studied the sensitivity of the results to the choice of the reggeon parameters α_1 and α_2 in (42), which control the diagonal and off-diagonal matrix elements, respectively. Variation of α_1 practically does not change the results. However, the dependence on α_2 is not negligible. The suppression of the off-diagonal $3q$-nucleon amplitudes in comparison with the diagonal ones is expected to be more strong for the reggeon exchange than for the Pomeron one. For this reason we chose for the upper bound of $|\alpha_2|$ the value 0.5, which is about the maximum value of $|\alpha_{pN}|$. The effect of variation of α_2 in the range (-0.5,0.5) for integrated nuclear transparency in the window $p_{m\perp}, |p_{m,z}| < 200$ MeV/c is illustrated in Fig. 15. As one can see, the positive values of α_2 decrease the nuclear transparency, and can to a certain extent obscure the CT effects at $Q^2 \lesssim 20$ GeV^2. In Figs. 16, 17 we demonstrate the effect of variation of α_2 for the unintegrated nuclear transparency for the parallel kinematics. It is seen that, the gross features of the $p_{m,z}$-dependence of the CT effect are stable with respect to variation of α_2. In the transverse kinematics the variation of α_2 yields only the overall renormalization of the nuclear transparency. Thus, as far as the F-B asymmetry of the nuclear transparency is concerned, the uncertainties of the reggeon amplitudes can not change the situation considerably. However, we are bound to conclude that at $Q^2 \lesssim 20$ GeV^2 the real situation may be more complicated for the observation of CT through Q^2-dependence of the integrated nuclear transparency.

In addition to the above discussion on the uncertainties of the theoretical predictions it is also appropriate to comment on the off-shell effects, which are neglected in our analysis. A successful observation of the missing momentum dependence of the CT effects is only

possible provided that the uncertainties of the missing momentum distribution extracted from the measured cross section of $(e, e'p)$ scattering are small in a comparison with the theoretically calculated contribution of the off-diagonal rescatterings. The determination of the missing momentum distribution includes the division of the experimental $(e, e'p)$ cross section by the half off-shell ep cross section. As a consequence, ambiguities in σ_{ep} lead to unavoidable uncertainties in the extracted missing momentum distribution. In order to estimate these uncertainties we compared the off-shell ep cross sections evaluated under different prescriptions discussed in ref. [23]. We found that the typical off-shell ambiguities are $\lesssim 5-10\%$ in the kinematical region considered in the present paper. Such uncertainties are not big enough to obscure the CT effects at $Q^2 \sim 10$ GeV^2 for the parallel kinematics, where CT effects increase the ratio $T_A(-p_{m,z}, p_{m\perp} = 0)/T_A(p_{m,z}, p_{m\perp} = 0)$ at $p_{m,z} \sim 250$ MeV/c by the factor ~ 2 (see Figs. 2, 3). At higher values of Q^2 ($\gtrsim 20$ GeV^2) the off-shell uncertainties can be neglected both for the parallel and transverse kinematics.

VI. CONCLUSIONS

We have studied the missing momentum dependence of the CT effects in $(e, e'p)$ scattering in the kinematical region of $p_m \lesssim 250$ MeV/c and $Q^2 \lesssim 40$ GeV^2. To perform such an analysis we developed a formalism based on the Glauber-Gribov multiple scattering theory. In our calculations we describe the target nucleus in the independent particle shell model. The formalism of CCMST was presented in the form which includes both the coherent and incoherent rescatterings. The coherent rescatterings describe FSI in exclusive $(e, e'p)$ reaction, when only the one-hole excitations of the target nucleus are allowed, while inclusion of both the coherent and incoherent rescatterings corresponds to inclusive experimental conditions involving all final states of the residual nucleus. The CT effects related to the incoherent rescattering were not considered in previous works.

We performed a qualitative analysis of the off-diagonal incoherent rescatterings mak-

ing use of the two-channel model. Our important observation is that, on the contrary to the case of coherent FSI, the contribution of the off-diagonal incoherent rescatterings does not vanish at small energies of the struck proton. For this reason, even at low Q^2, in the case of the inclusive reaction the Glauber model becomes unreliable for treatment of FSI in the region of large missing momenta, where the incoherent rescatterings dominate. We demonstrated that CT leads to a decrease of the contribution of the incoherent rescatterings and a conspiracy of the CT effects from the coherent and incoherent rescatterings may take place in measurement of the integrated nuclear transparency. We argue that this phenomenon may be important in $(p, 2p)$ scattering, where the contribution of the incoherent rescatterings are enhanced in a comparison with $(e, e'p)$ reaction.

The numerical calculations of the present paper were carried out for the exclusive $(e, e'p)$ reaction. In the region of $p_m \lesssim 150-200$ MeV/c, where the effect of the incoherent FSI becomes small, our predictions can be compared with the experimental data obtained in inclusive $(e, e'p)$ reaction. Our calculations show that at $Q^2 \lesssim 5$ GeV^2 the CT effects are still small in the whole missing momentum region considered in the present paper. At $Q^2 \sim 10$ GeV^2 we find a considerable CT effect only in the case of the parallel kinematics in the region of $p_{m,z} \sim -(200 - 250)$ MeV/c. The CT increases the ratio $T_A(-p_{m,z}, p_{m\perp} = 0)/T_A(p_{m,z}, p_{m\perp} = 0)$ at $p_{m,z} \sim 250$ MeV/c by the factor ~ 2. This effect is stronger for the light target nuclei. It could be observed in a high precision experiment. Our calculations show that the developed CT regime starts with $Q^2 \sim 40$ GeV^2, where the CT effects change the missing momentum distribution drastically.

We studied for the first time the impact of the reggeon exchanges on the CT effects. It was found that in the region of $Q^2 \lesssim 40$ GeV^2 the effect of the diagonal $3q$-nucleon reggeon amplitudes is practically saturated by the elastic $pN \to pN$ amplitude. However, the off-diagonal resonance-nucleon reggeon amplitudes may be important. We found that the onset of the CT regime for integrated nuclear transparency may be delayed if the reggeon exchanges generates the positive value of the Re/Im ratio for the off-diagonal amplitudes.

None the less the CT effect in the F-B asymmetry is insensitive to the reggeon amplitudes.

For the first time we presented a detailed analysis of the convergence of the CCMST series in the number of the included resonance states. Our results indicate that at $Q^2 \lesssim 40$ GeV^2 the first 2-3 excited states practically saturate the contribution of the off-diagonal rescatterings in exclusive $(e, e'p)$ scattering.

The results obtained for the integrated nuclear transparency show that the observation of CT through the Q^2-dependence of the integrated nuclear transparency is hardly possible at $Q^2 \lesssim 10$ GeV^2. However, extension of the kinematical region up to $Q^2 \sim 40$ GeV^2 could provide the observation of CT if the small-size $3q$ configurations actually dominate in hard ep scattering.

ACKNOWLEDGMENTS

This work was partly supported by the Grant N9S000 from the International Science Foundation and the INTAS grant 93-239. AAU acknowledges Prof. A. Zichichi and ICSC- World Laboratory for financial support. BGZ wishes to gratefully acknowledge the hospitality of the Interdisciplinary Laboratory of SISSA and the Institut für Kernphysik, KFA, Jülich.

REFERENCES

[1] S.J.Brodsky and G.P.Lepage, Phys. Rev. **D22** (1980) 2157.

[2] A.H.Mueller, *in: Proceedings of the XVII Rencontre de Moriond, Les Arcs, France.* Ed. Tranh Thanh Van, Editions Frontieres, Gif-sur-Yvette, 1982, p.13.

[3] S.J.Brodsky, *in: Proceedings of the XIII International Symposium on Multiparticle Dynamics, Volendam, Netherlands.* Eds. E.W.Kittel, W.Metzger and A.Stergion, World Scientific, Singapore, 1982, p. 963.

[4] R.J.Glauber, in: *Lectures in Theoretical Physics*, v.1, ed. W.Brittain and L.G.Dunham. Interscience Publ., N.Y., 1959; R.J.Glauber and G.Matthiae, Nucl. Phys. **B21** (1970) 135.

[5] V.N.Gribov, Sov. Phys. JETP **29** (1969) 483; **30** (1970) 709.

[6] N.N.Nikolaev, A.Szczurek, J.Speth, J.Wambach, B.G.Zakharov and V.R.Zoller, Nucl. Phys. **A567** (1994) 781.

[7] A.Bianconi, S.Boffi, and D.E.Kharzeev, Nucl. Phys. **A565** (1993) 767.

[8] B.K.Jennings and B.Z.Kopeliovich, Phys. Rev. Lett. **70** (1993) 3384

[9] N.N.Nikolaev, A.Szczurek, J.Speth, J.Wambach, B.G.Zakharov and V.R.Zoller, Phys. Lett. **B317** (1993) 287.

[10] A.Bianconi, S.Boffi, and D.E.Kharzeev, Phys. Lett. **B325** (1994) 294.

[11] A.Kohama and K.Yazaki, Nucl. Phys. **A575** (1994) 645.

[12] A.Kohama, K.Yazaki and R.Seki, Phys. Lett. **B344** (1995) 61.

[13] B.Z.Kopeliovich and B.G.Zakharov, Phys. Rev. **D44** (1991) 3466.

[14] B.Z.Kopeliovich and B.G.Zakharov, Phys. Lett. **B264** (1991) 434.

[15] NE18 Collaboration: N.C.R.Makins et al., Phys. Rev. Lett. **72** (1994) 1986; T.G. O'Neill et al., Phys. Lett. **B351** (1995) 93.

[16] O. Benhar *et al.*, Phys. Rev. C **44** (1991) 2328.

[17] N.N.Nikolaev, J.Speth, B.G.Zakharov, Jülich preprint **KFA-IKP(Th)-1995-01**, January 1995, submitted to Nucl. Phys. **A**.

[18] O.Benhar, S.Fantoni, N.N.Nikolaev, J.Speth, A.A.Usmani and B.G.Zakharov, Phys. Lett. **B358** (1995) 191.

[19] J.W. Van Orden, W. Truex and M.K. Banerjee, Phys. Rev. **C21** (1980) 2628; S. Fantoni and V.R. Pandharipande, Nucl. Phys. **A427** (1984) 473.

[20] S.C.Pieper, R.B.Wiringa and V.R.Pandharipande, Phys. Rev. C46 (1992) 1741.

[21] A.Bianconi, S.Jeschonnek, N.N.Nikolaev and B.G.Zakharov, Jülich preprint **KFA-IKP(Th)-1995-13**, March 1995, submitted to Nucl. Phys. **A**.

[22] F.F.Frankfurt, M.I.Strikman and M.B.Zhalov, Nucl. Phys. **A515** (1990) 599.

[23] T. de Forest Jr., Nucl. Phys. **A392** (1983) 232.

[24] S.Frullani and J.Mourgey, Adv. Nucl. Phys., Editors J.W.Negele and E.Vogt **14** (1984) 3.

[25] S.Boffi, C.Giusti and F.D.Pacati, Phys. Rep. **226** (1993) 1.

[26] G.D.Alkhazov, S.I.Belostotsky and A.A.Vorobyev, Phys. Rep. **C42** (1978) 89.

[27] B.G.Zakharov, Sov. J. Nucl. Phys. **46** (1987) 92.

[28] F.Low, Phys. Rev. **D12** (1975) 163; S.Nussinov, Phys. Rev. Lett. (1975) 1286.

[29] B.Z.Kopeliovich and B.G.Zakharov, Sov. J. Nucl. Phys. **46** (1987) 911.

[30] N.N.Nikolaev and B.G.Zakharov, Z.f.Phys. **C49** (1991) 607.

[31] N.N.Nikolaev and B.G.Zakharov, Z.f.Phys. **C53** (1992) 331.

[32] N.N.Nikolaev and B.G.Zakharov, to be published in Proceedings of the International Nuclear Physics Conference, August 21-26, 1995, Beijing, China.

[33] G.Alberi and G.Goggi, Phys. Rep. **74** (1981) 1.

[34] J.Nemchik, N.N.Nikolaev and B.G.Zakharov, Proceedings of the Workshop on CEBAF at Higher Energies, CEBAF, April 14-16, 1994, Editors: Nathan Isgur and Paul Stoler, pp. 415-464.

[35] G.Cohen-Tannoudji, A.E.Hassouni, J.Kalinowski, R.Peschanski, Phys. Rev. **D19** (1979) 3397; A.Capella, J.Tran Thanh Van, Phys. Lett. **B114** (1982) 450; A.B.Kaidalov, Phys.Lett. **B116** (1982) 459.

[36] N.N.Nikolaev, JETP Lett. **57** (1993) 85.

[37] H. de Vries et al., Atomic Data and Nuclear Data Tables **36** (1987) 496.

[38] O.Benhar, C.Ciofi Degli Atti, S.Liuti and G.Salme, Phys. Lett.**B177** (1986) 135.

[39] C.Lechanoine-LeLuc and F.Lehar, Rev. Mod. Phys. **65** (1993) 47.

FIGURES

FIG. 1. The typical diagrams contributing to the operator $\hat{U}(\vec{r}_1, \vec{r}_1^{\,'})$ describing the evolution of the density matrix of $3q$ ejectile state within CCMST: (a) the diagram without the interaction between the two trajectories outgoing from $\vec{r}_1$ and $\vec{r}_1^{\,'}$, (b) the diagram containing the interaction between the trajectories generated by the $\hat{\Gamma}\hat{\Gamma}^*$ term in Eq. (23). The dotted lines attached to the straight-line trajectory originating from $\vec{r}_1(\vec{r}_1^{\,'})$ denote a profile function $\hat{\Gamma}(\vec{b}_j - \vec{b}_1, z_j - z_1)(\hat{\Gamma}^*(\vec{b}_j - \vec{b}_1^{\,'}, z_j - z_1^{'}))$.

FIG. 2. Nuclear transparency in exclusive $^{16}O(e, e'p)$ scattering in parallel kinematics $p_{m\perp} = 0$ calculated within CCMST (solid curve) and in the Glauber model (dotted curve).

FIG. 3. The same as Fig. 2, but for $^{40}Ca(e, e'p)$ scattering.

FIG. 4. Nuclear transparency in exclusive $^{16}O(e, e'p)$ scattering in transverse kinematics $p_{m,z} = 0$ calculated within CCMST (solid curve) and in the Glauber model (dotted curve).

FIG. 5. The same as Fig. 4, but for $^{40}Ca(e, e'p)$ scattering.

FIG. 6. The Q^2-dependence of nuclear transparency for exclusive $^{16}O(e, e'p)$ scattering at different windows D in the transverse and longitudinal missing momentum obtained within CCMST (solid curve) and in the Glauber model (dotted curve).

FIG. 7. The same as Fig. 6, but for $^{40}Ca(e, e'p)$ scattering.

FIG. 8. The Q^2-dependence of nuclear transparency for exclusive $^{16}O(e, e'p)$ scattering for excitations of the separate hole states at the kinematical window $p_{m\perp}$, $|p_{m,z}| < 200$ MeV/c obtained within CCMST (solid curve) and in the Glauber model (dotted curve).

FIG. 9. The same as Fig. 8, but for $^{40}Ca(e, e'p)$ scattering.

FIG. 10. The missing momentum distribution for $^{16}O(e, e'p)$ scattering in parallel kinematics $p_{m\perp} = 0$ for the separate shells calculated within CCMST (solid curve) and in the Glauber model (dotted curve). The dot-dashed curve shows the SPMD.

FIG. 11. The same as Fig. 10, but for $^{40}Ca(e, e'p)$ scattering.

FIG. 12. The same as Fig. 10, but for transverse kinematics.

FIG. 13. The same as Fig. 11, but for transverse kinematics.

FIG. 14. The convergence of CCMST expectation for nuclear transparency in exclusive $^{16}O(e,e'p)$ and $^{40}Ca(e,e'p)$ scattering for the missing momentum window $p_{m\perp},\ |p_{m,z}| < 200$ Mev/c with respect to the number of the $3q$ states included: $n = 1$ (solid curve), $n = 2$ (long-dashed curve), $n = 3$ (dot-dashed curve), $n = 4$ (dotted curve).

FIG. 15. Nuclear transparency for exclusive $^{16}O(e,e'p)$ and $^{40}Ca(e,e'p)$ scattering for the missing momentum window $p_{m\perp},\ |p_{m,z}| < 200$ Mev/c calculated within CCMST with different sets of the reggeon parameters: $\alpha_2 = 0$ (solid curve), $\alpha_2 = -0.5$ (long-dashed curve), $\alpha_2 = 0.5$ (short-dashed curve), in all the cases $\alpha_1 = 1$. The predictions of the Glauber model are shown by the dotted curve.

FIG. 16. The $p_{m,z}$-dependence of the nuclear transparency for exclusive $^{16}O(e,e'p)$ scattering. The legend of curves is the same as in Fig. 15.

FIG. 17. The same as Fig. 16, but for $^{40}Ca(e,e'p)$ scattering.

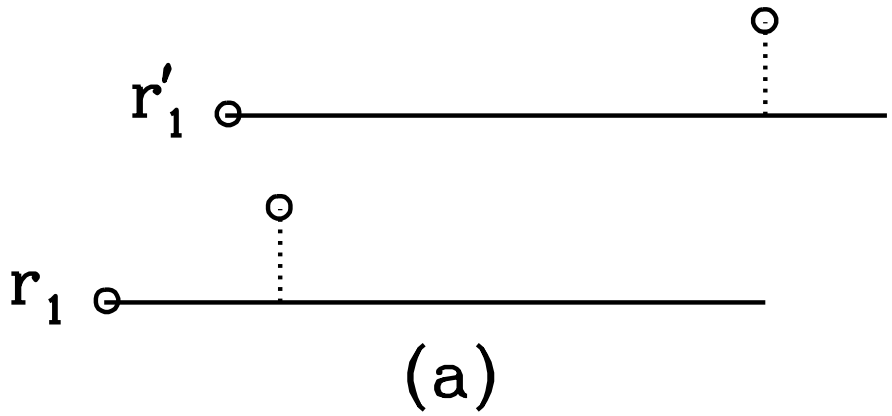

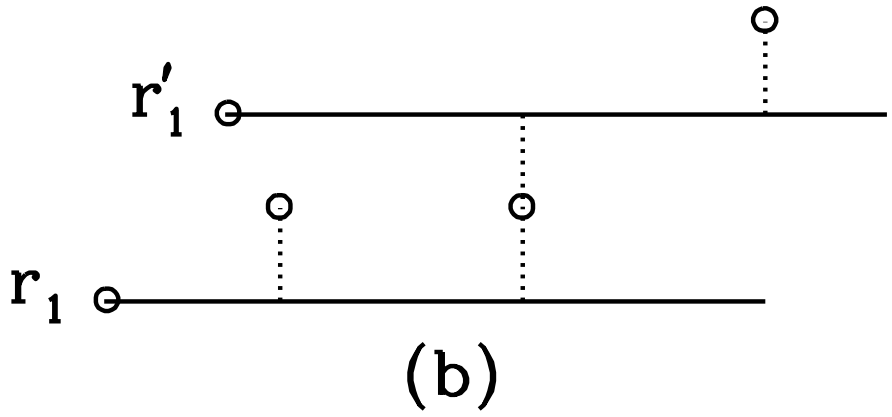

fig1. O. Benhar et. al.

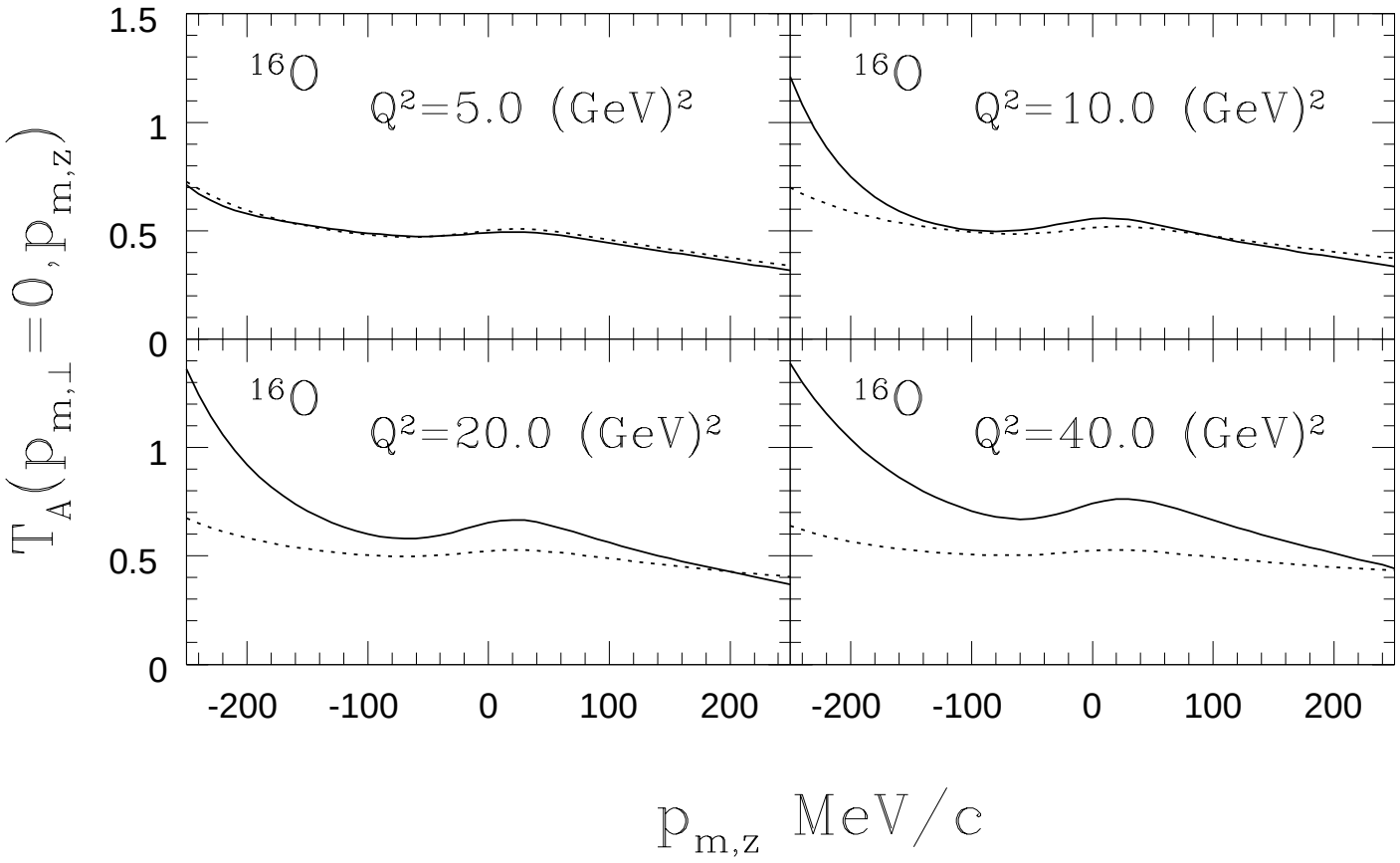

fig2. O. Benhar et. al.

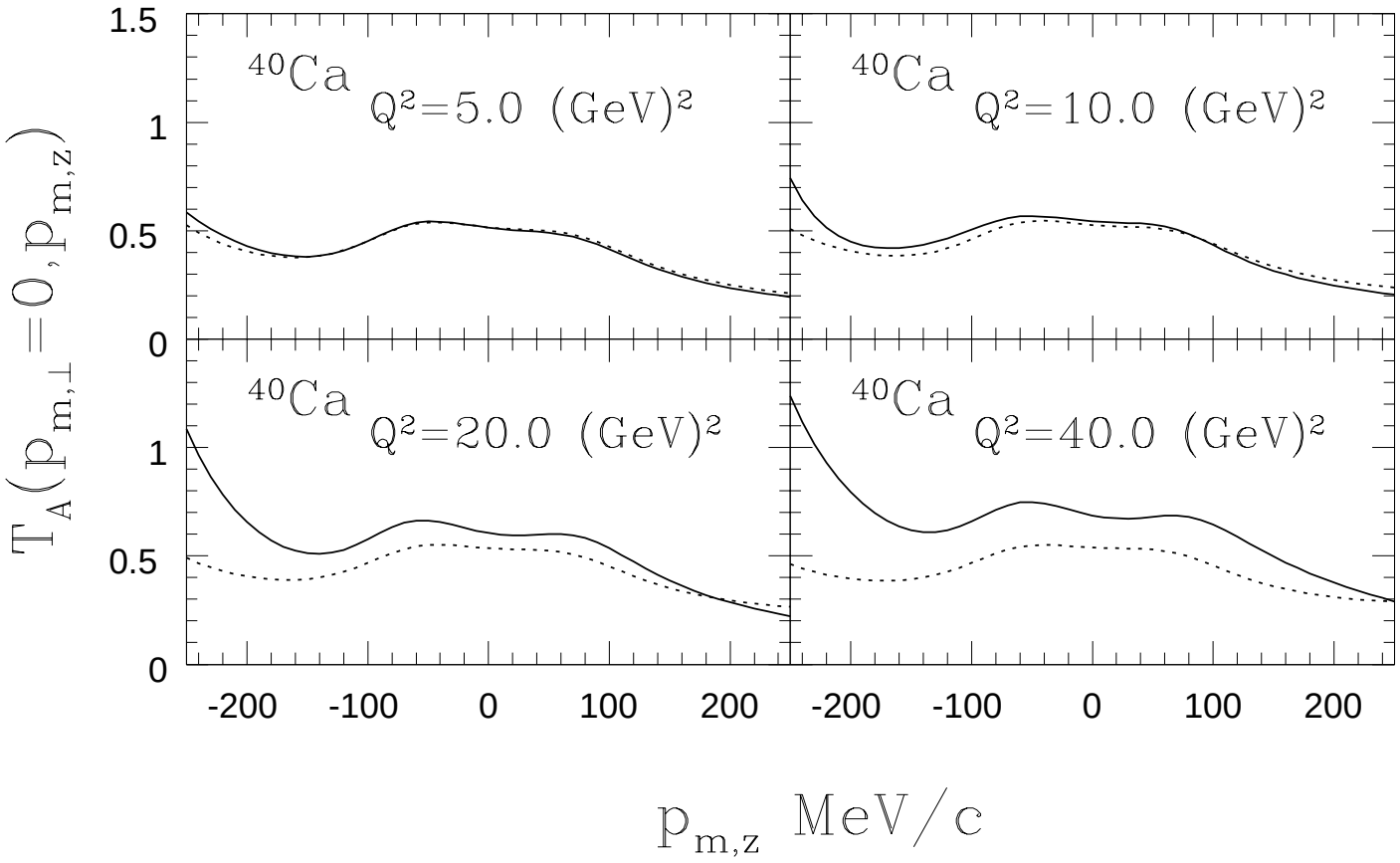

fig3. O. Benhar et. al.

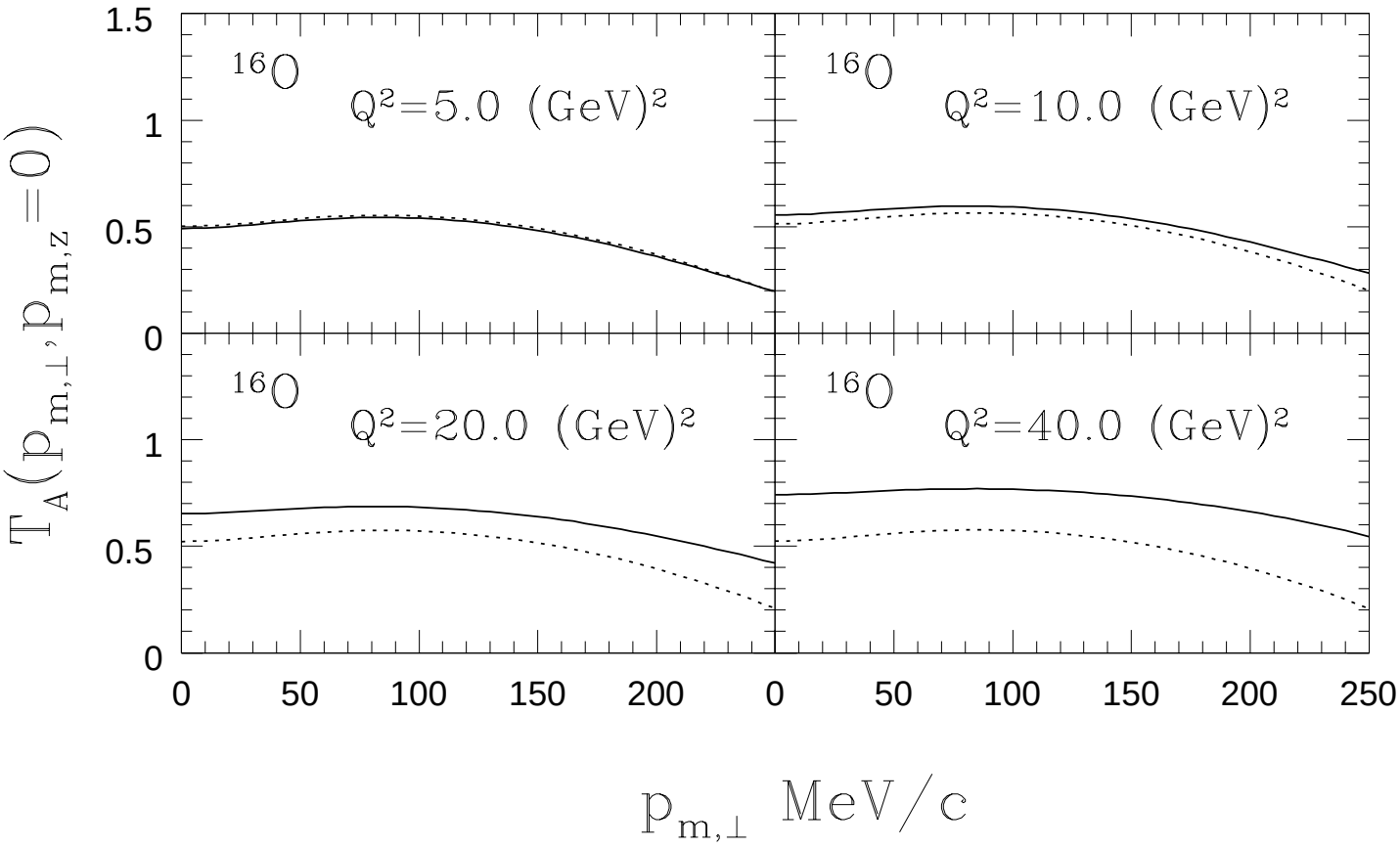

fig4. O. Benhar et. al.

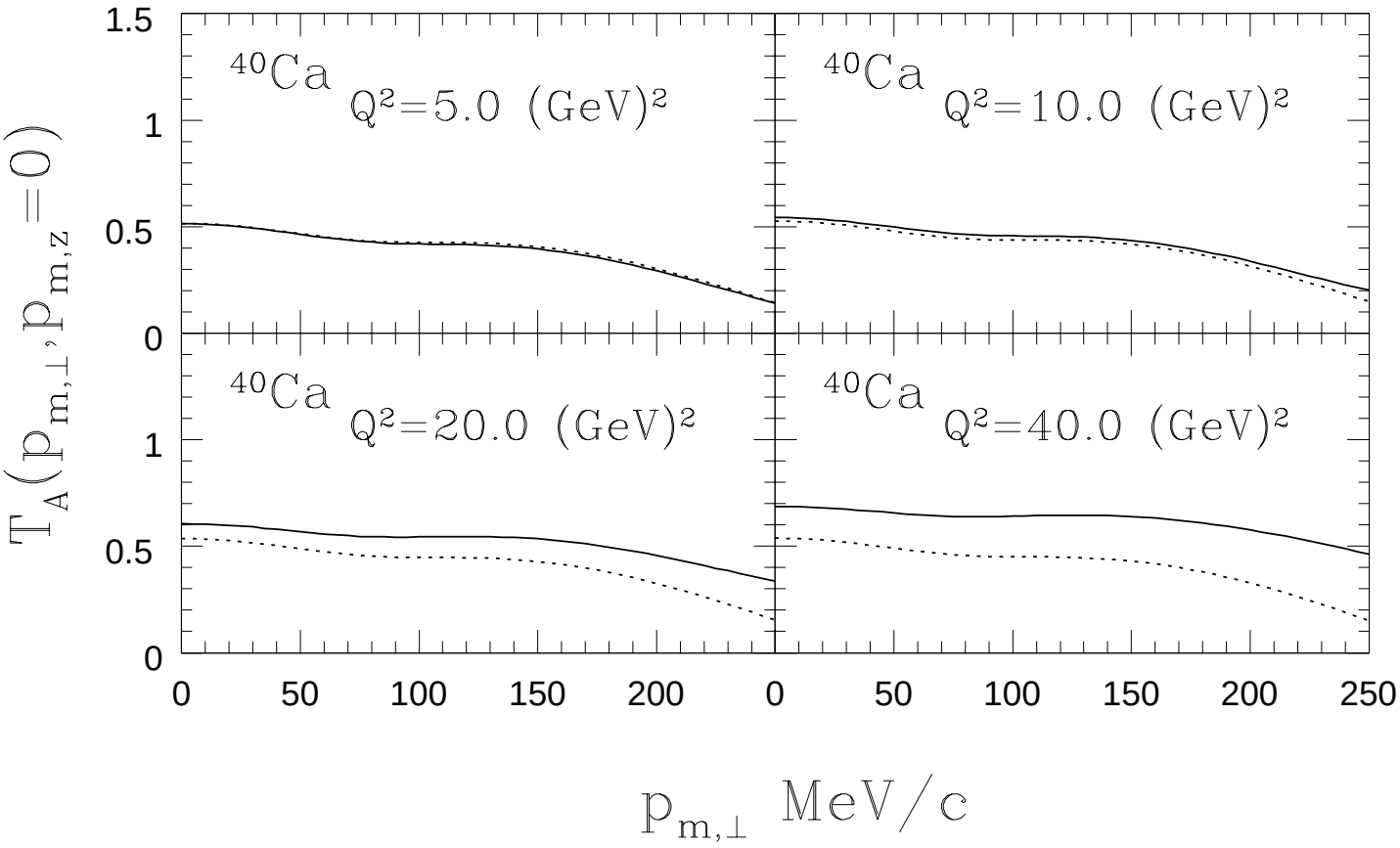

fig5. O. Benhar et. al.

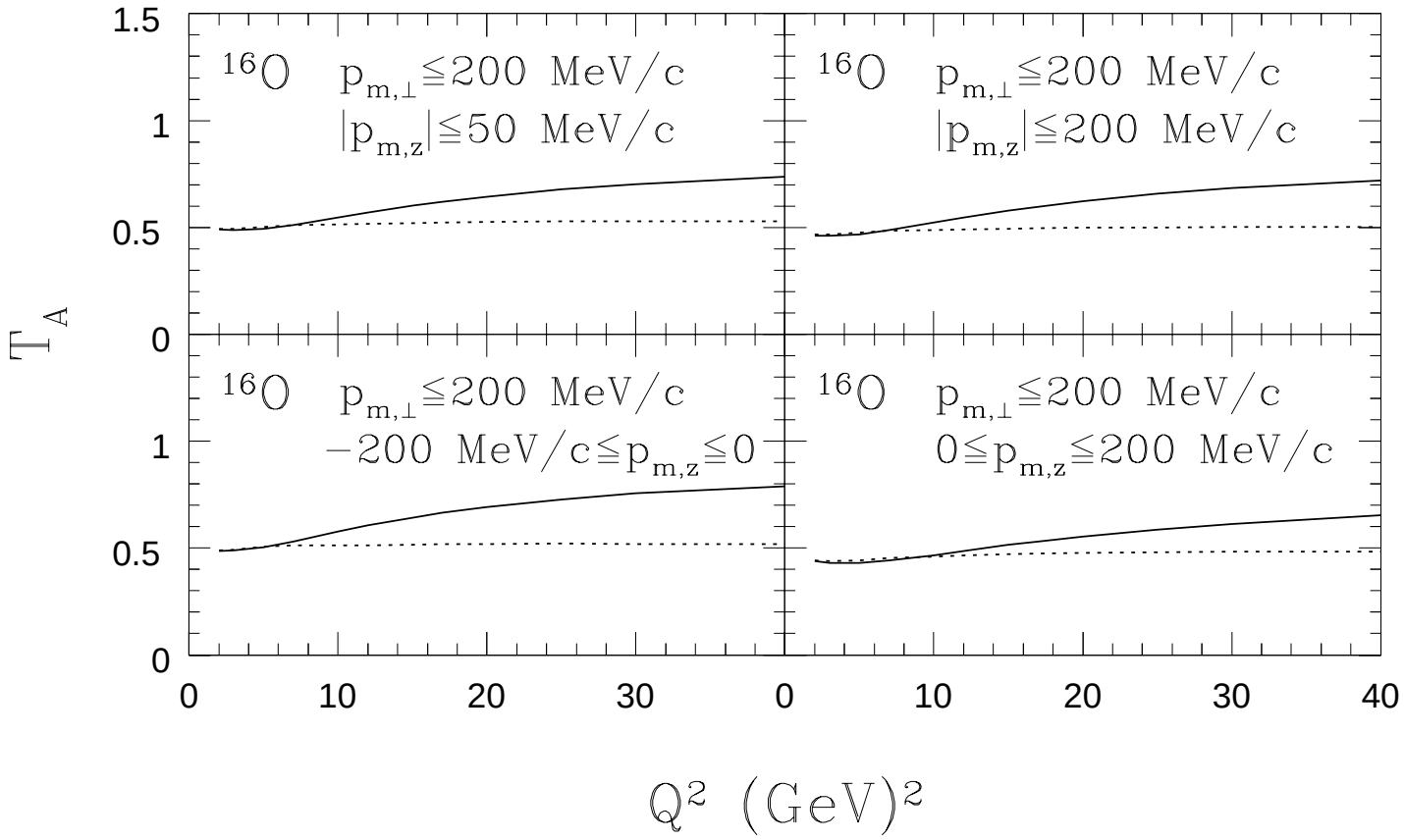

fig6. O. Benhar et. al.

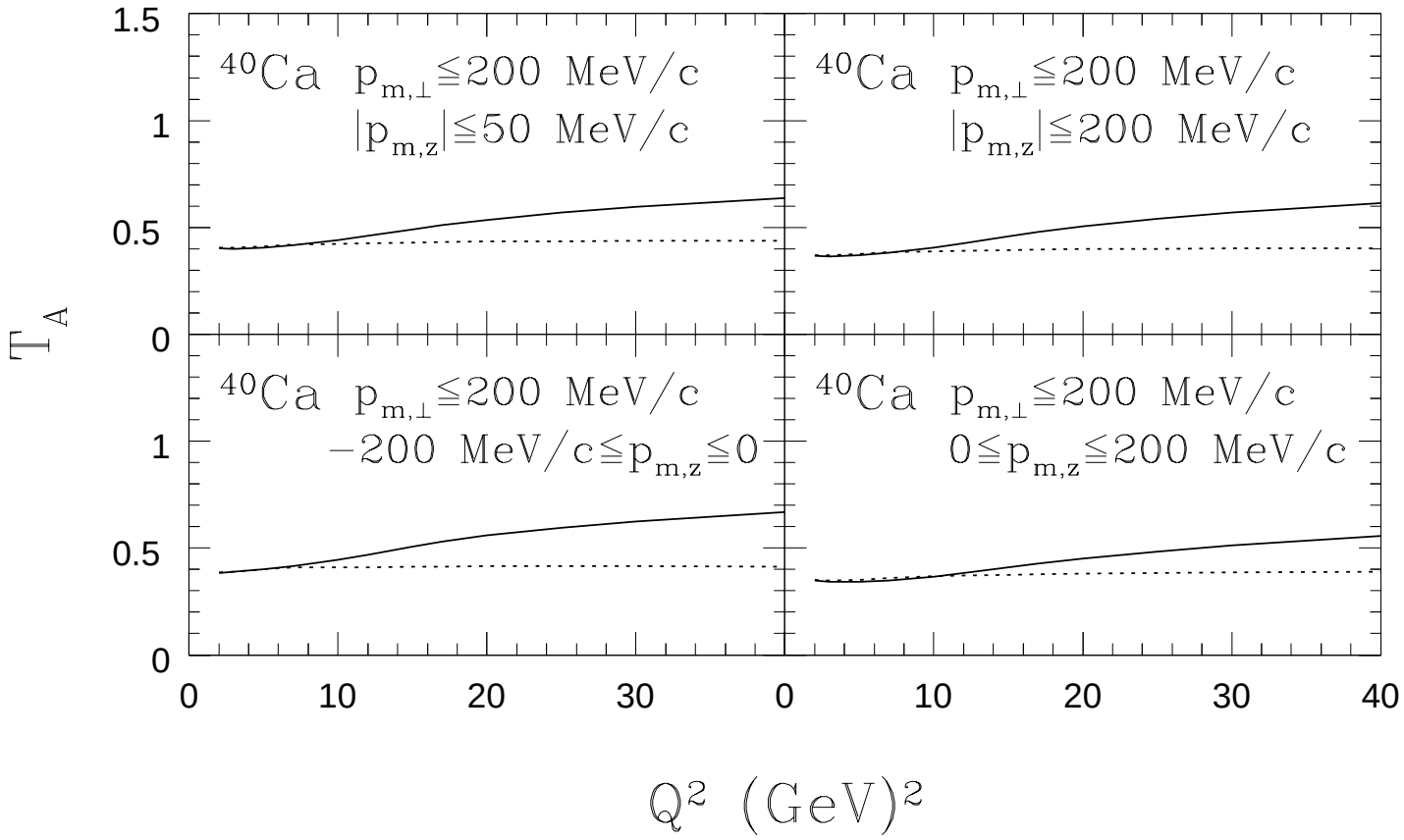

fig7. O. Benhar et. al.

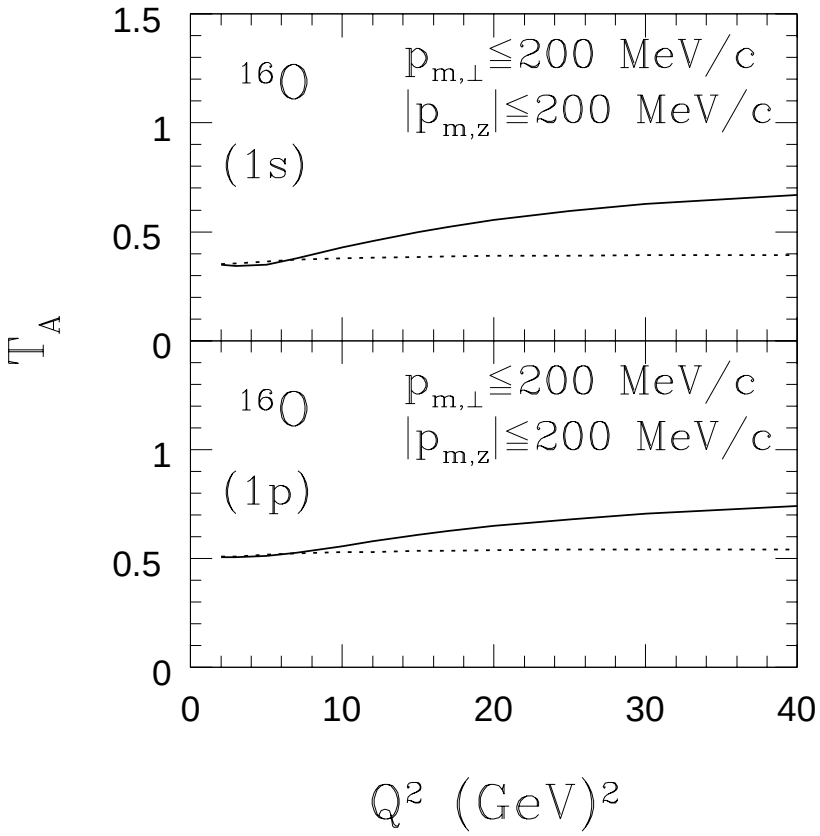

fig8. O. Benhar et. al.

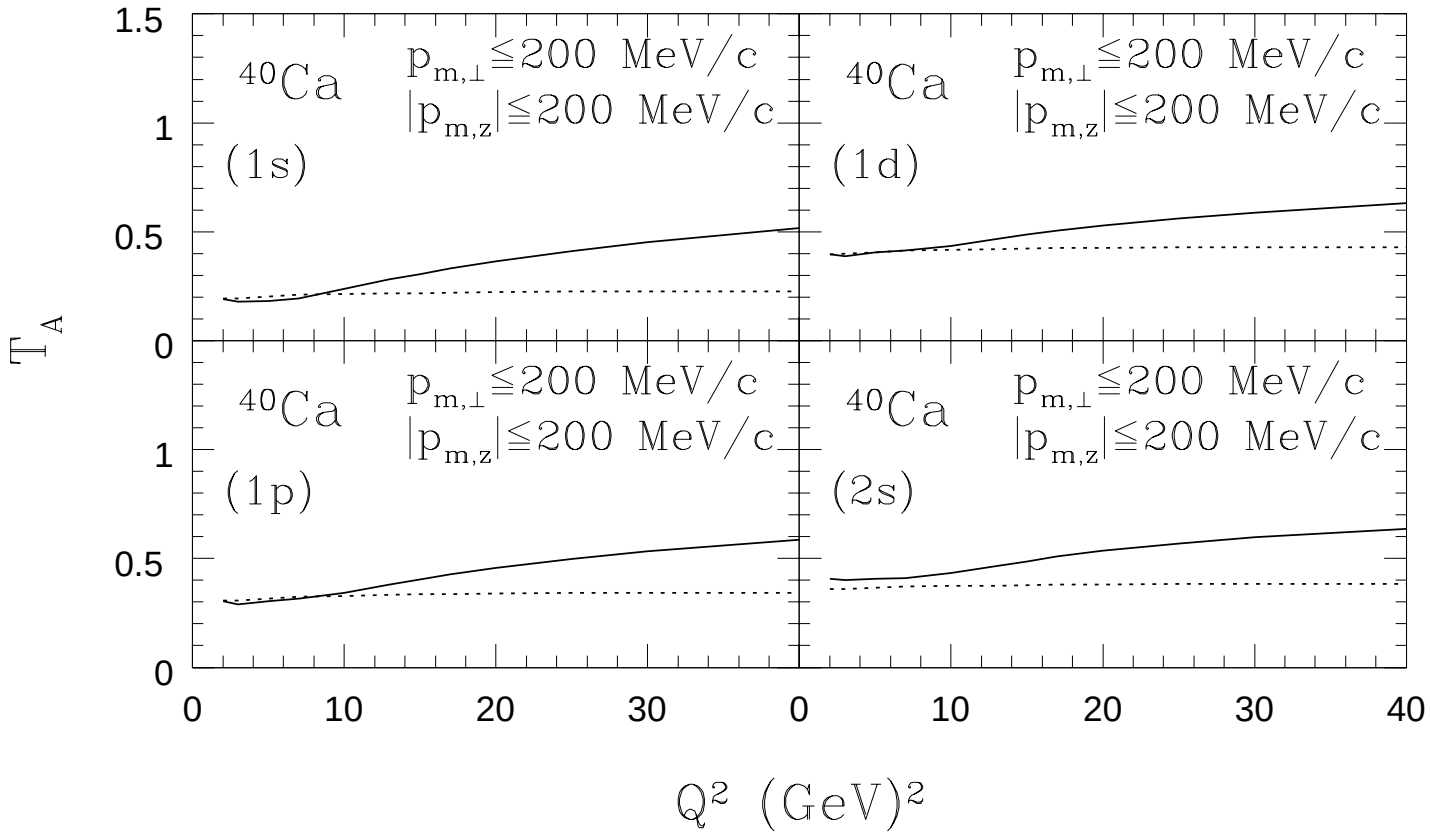

fig9. O. Benhar et. al.

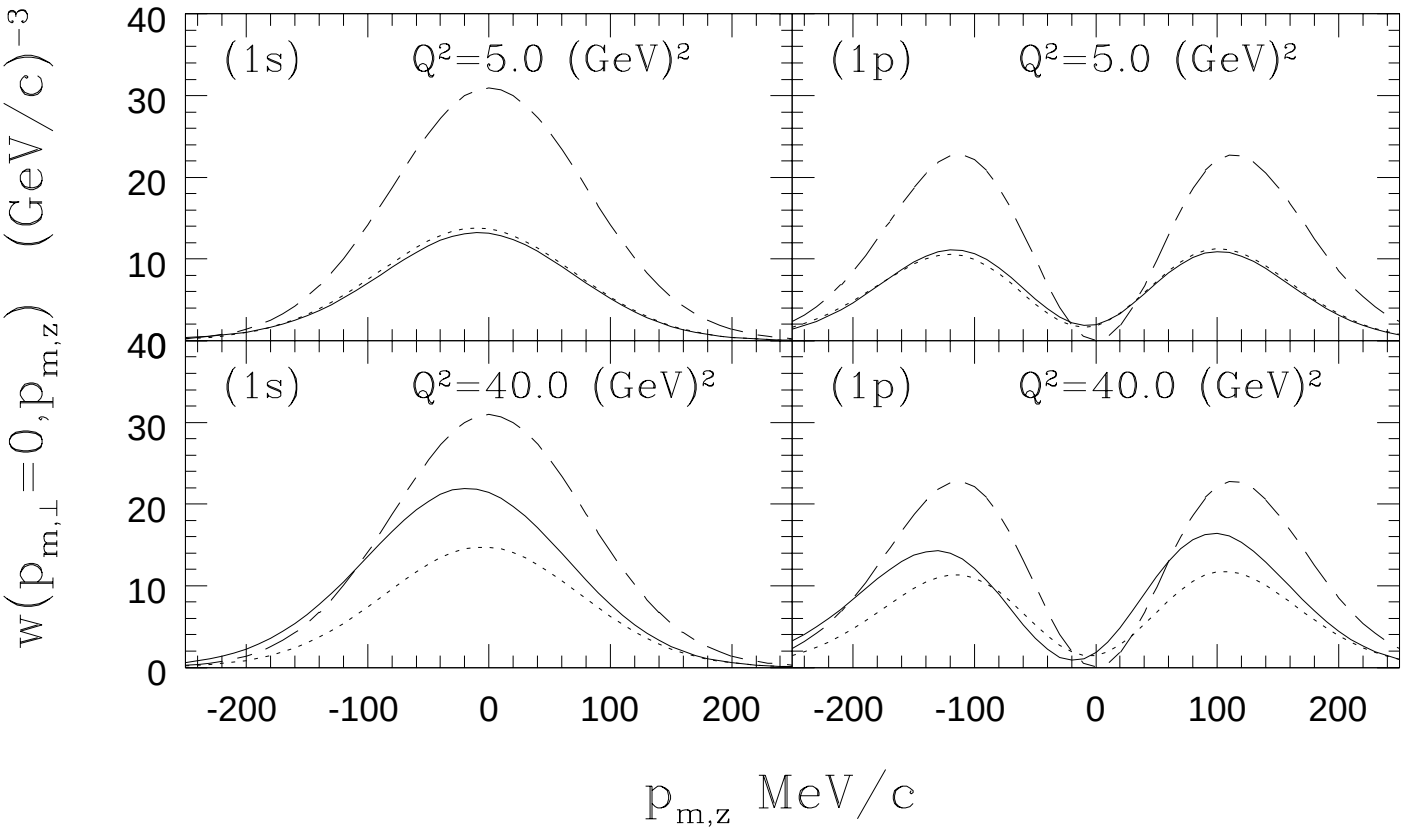

fig10. O. Benhar et. al.

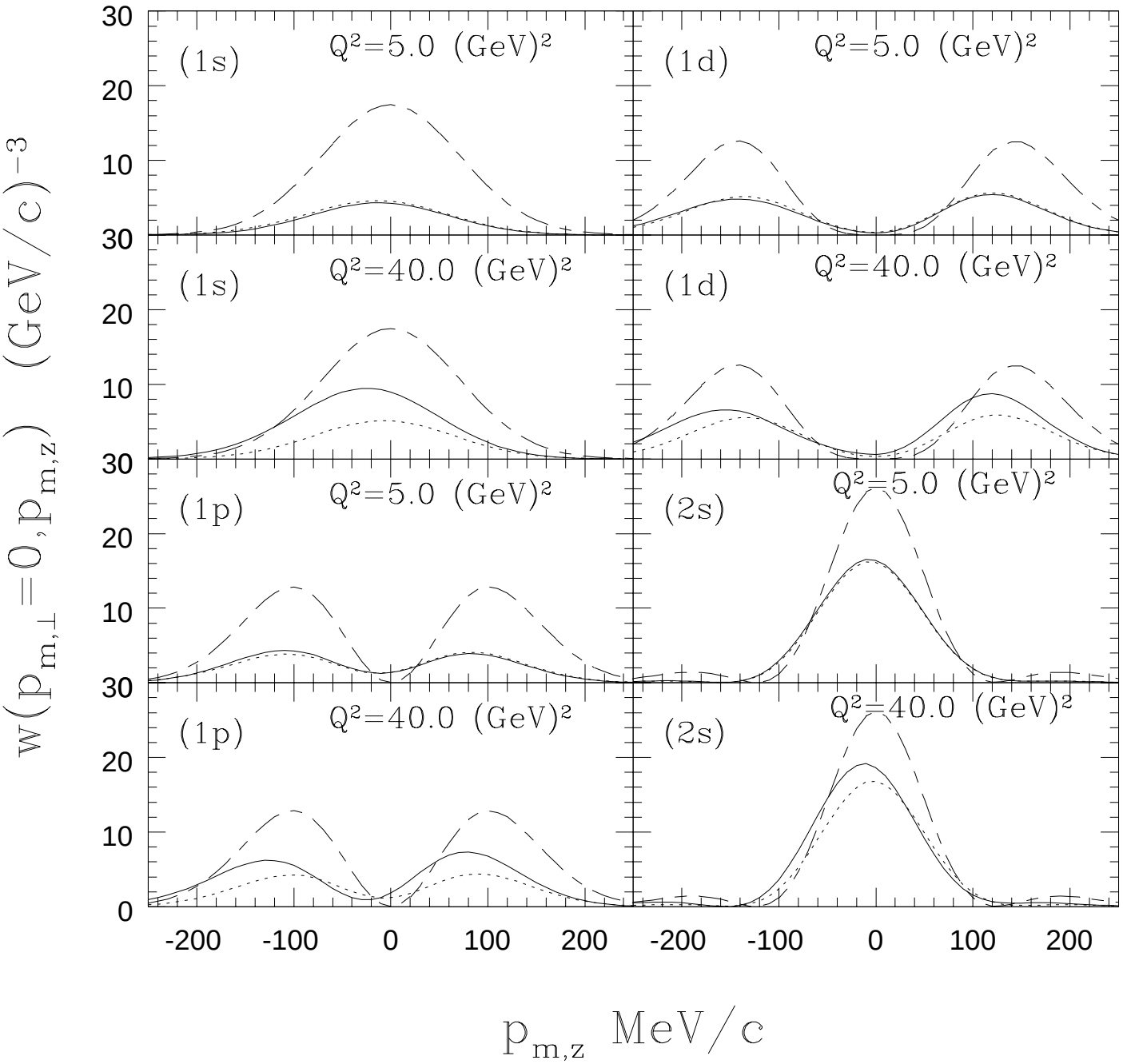

fig11. O. Benhar et. al.

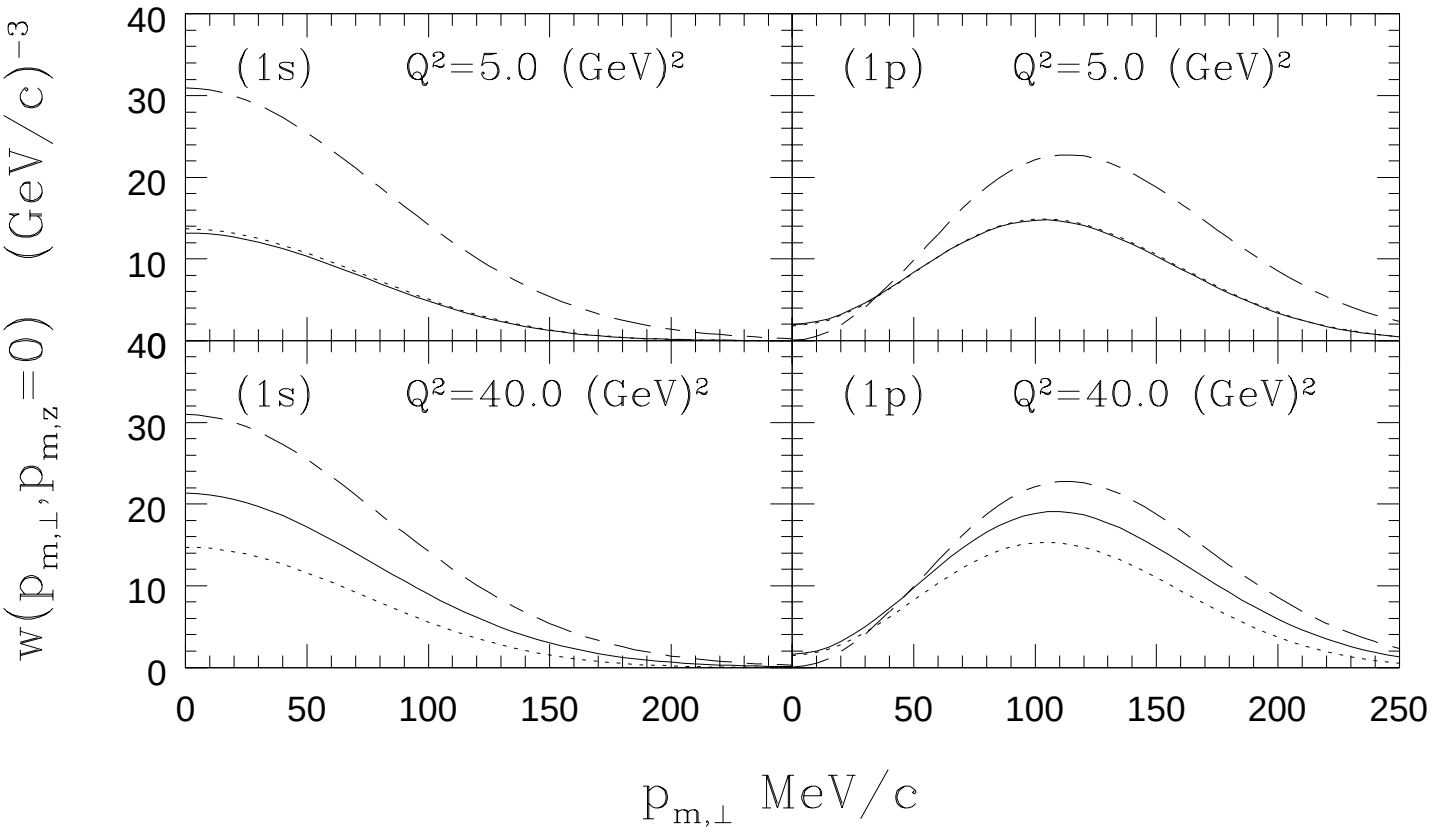

fig12. O. Benhar et. al.

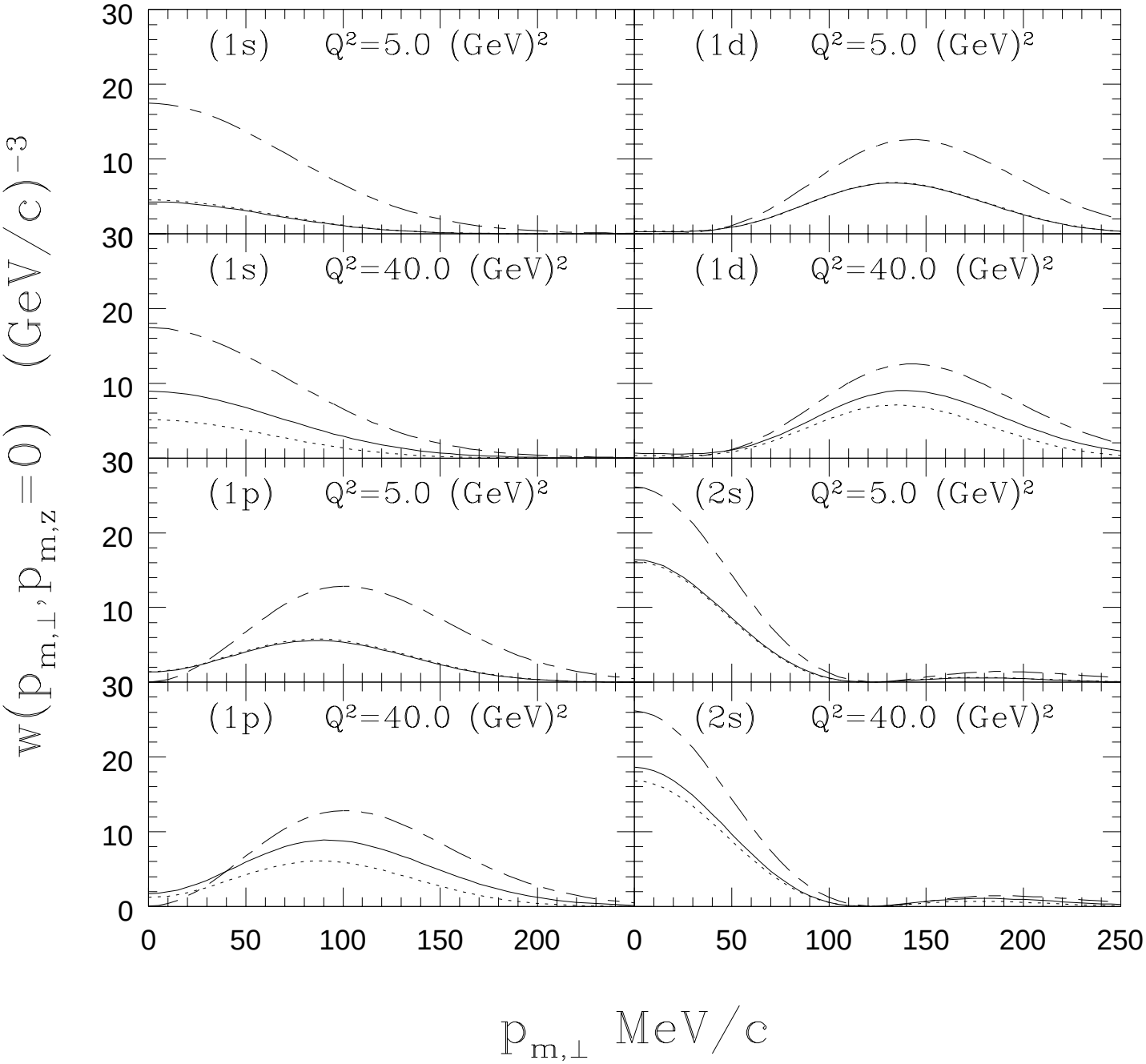

fig13. O. Benhar et. al.

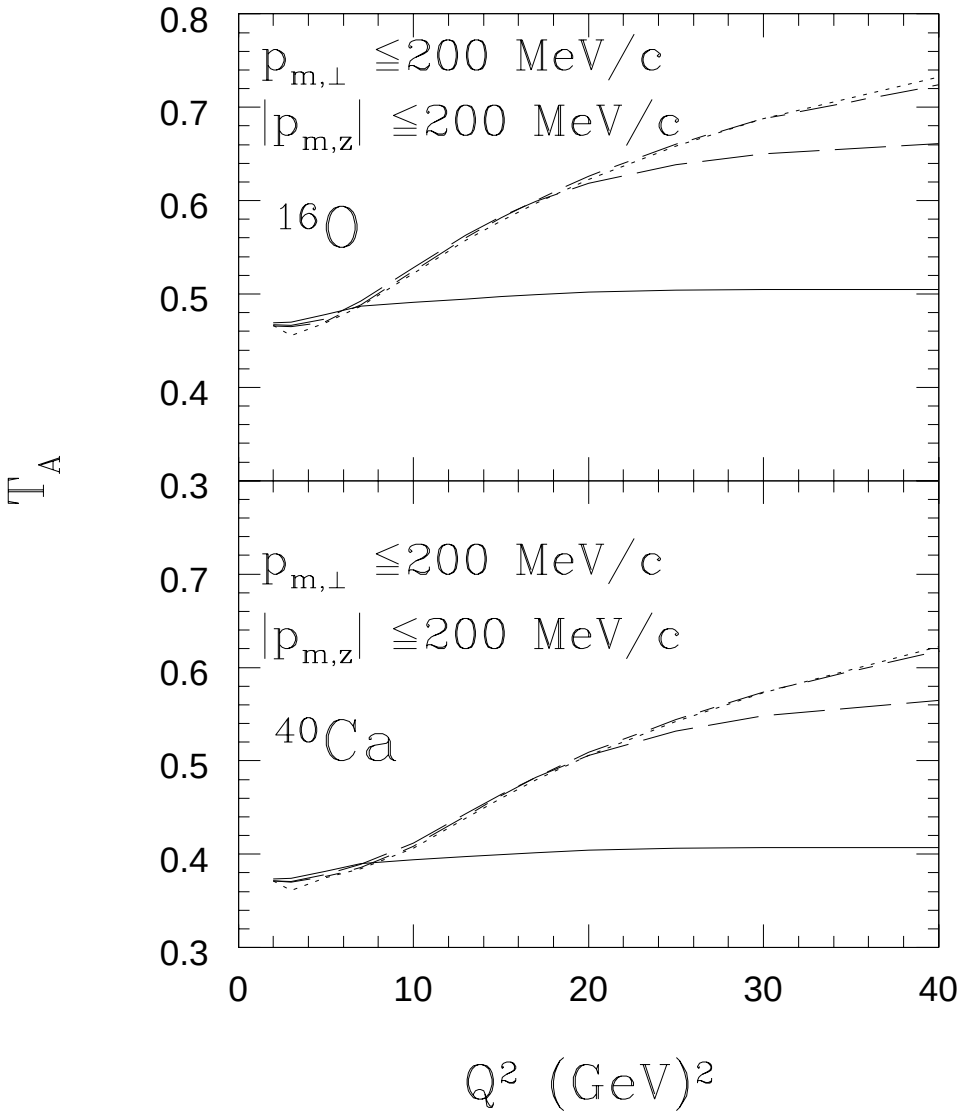

fig14. O. Benhar et. al.

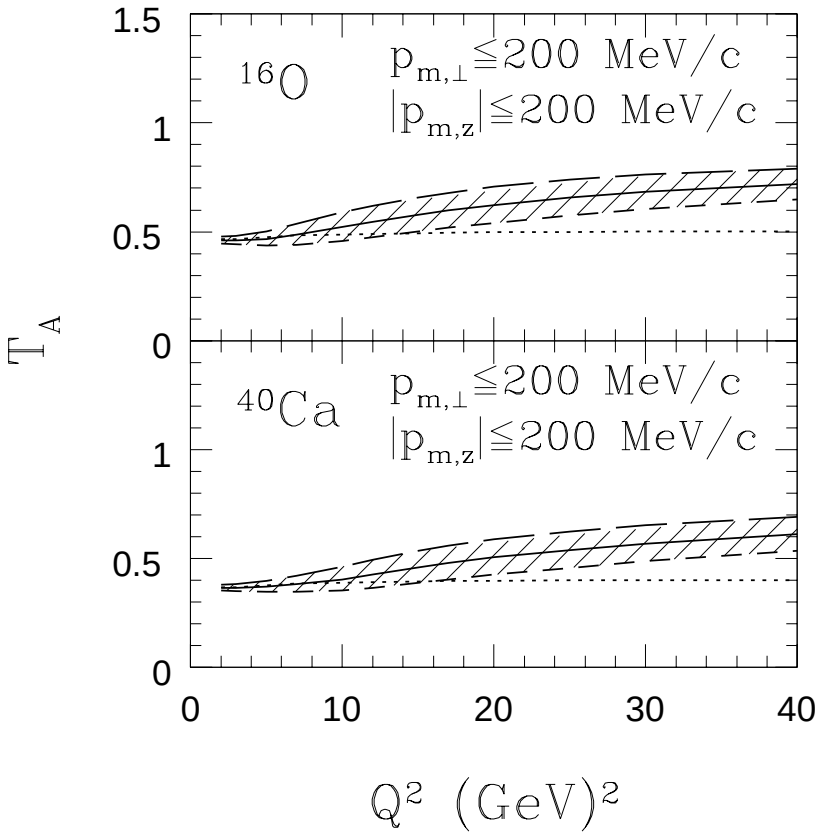

fig15. O. Benhar et. al.

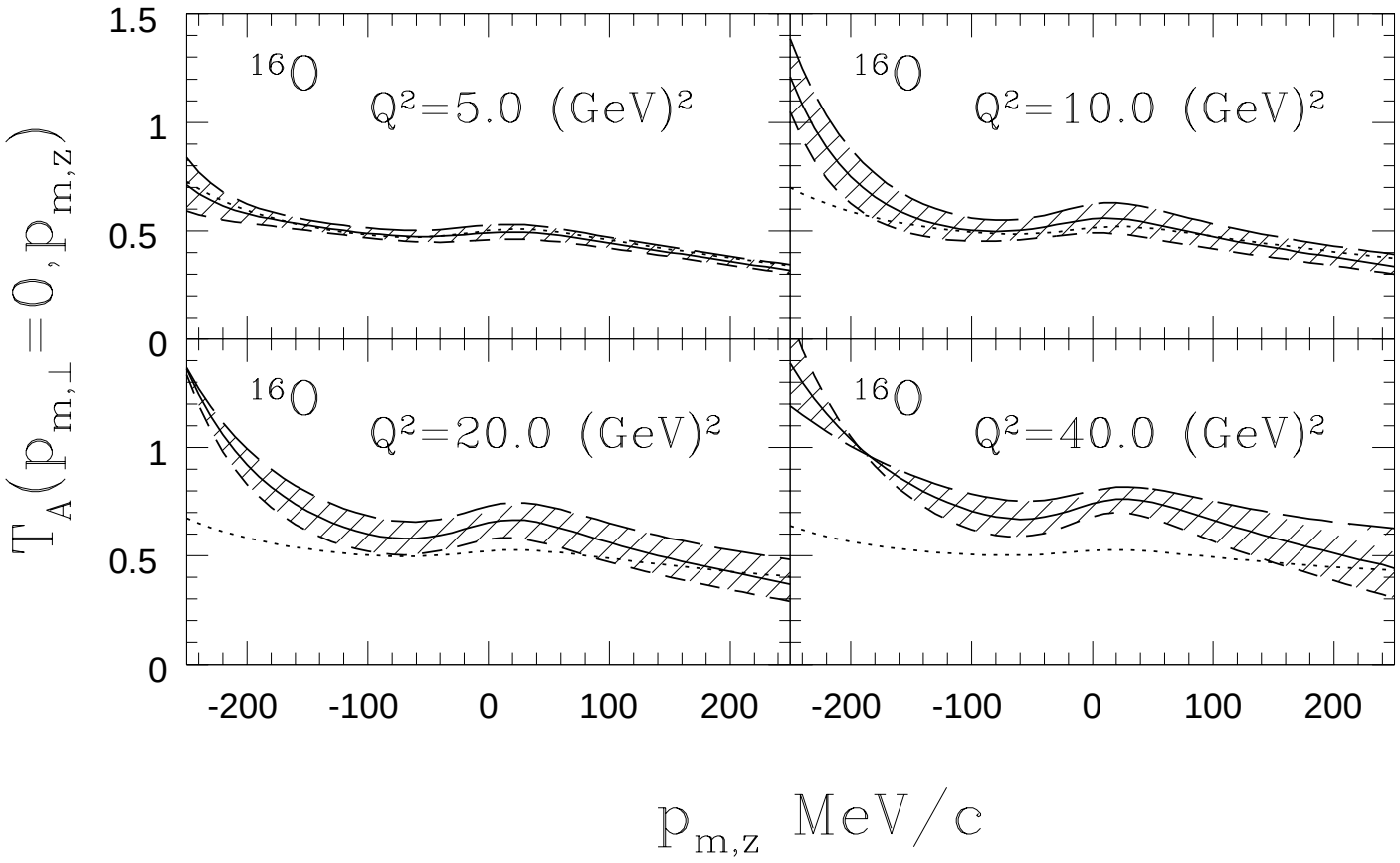

fig16. O. Benhar et. al.

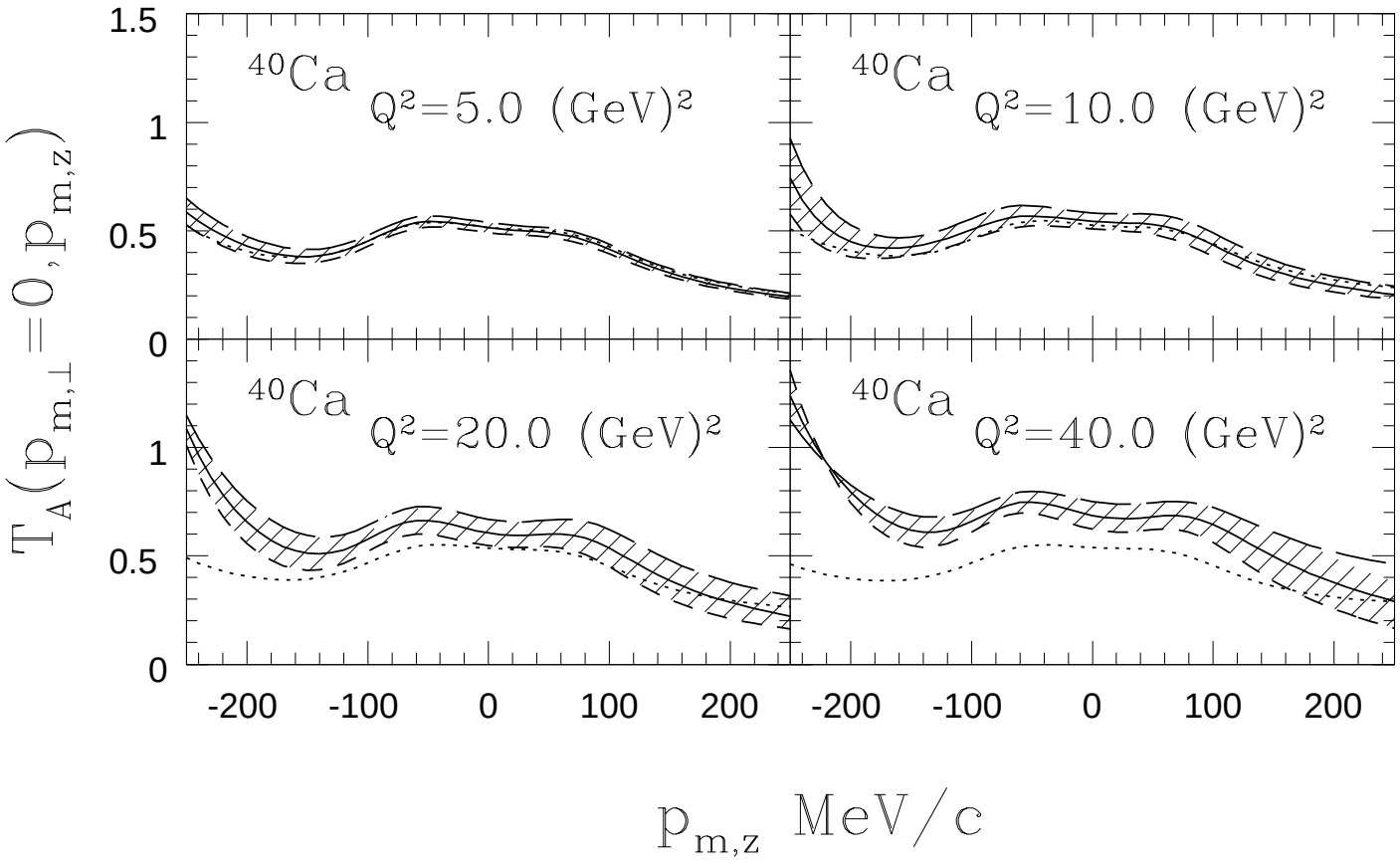

fig17. O. Benhar et. al.